Comparison of age distributions estimated from environmental tracers by using binary-dilution and numerical models of fractured and folded karst: Shenandoah Valley of Virginia and West Virginia, USA

Richard M. Yager · L. Niel Plummer · Leon J. Kauffman · Daniel H. Doctor · David L. Nelms · Peter Schlosser

Abstract Measured concentrations of environmental tracers in spring discharge from a karst aquifer in the Shenandoah Valley, USA, were used to refine a numerical groundwater flow model. The karst aquifer is folded and faulted carbonate bedrock dominated by diffuse flow along fractures. The numerical model represented bedrock structure and discrete features (fault zones and springs). Concentrations of ^{3}H, ^{3}He, ^{4}He, and CFC-113 in spring discharge were interpreted as binary dilutions of young (0–8 years) water and old (tracer-free) water. Simulated mixtures of groundwater are derived from young water flowing along shallow paths, with the addition of old water flowing along deeper paths through the model domain that discharge to springs along fault zones. The simulated median age of young water discharged from springs (5.7 years) is slightly older than the median age estimated from $^{3}H/^{3}He$ data (4.4 years). The numerical model predicted a fraction of old water in spring discharge (0.07) that was half that determined by the binary-dilution model using the $^{3}H/^{3}He$ apparent age and ^{3}H and CFC-113 data (0.14). This difference suggests that faults and lineaments are more numerous or extensive than those mapped and included in the numerical model.

Keywords Groundwater age · Fractured rocks · Karst · Numerical modelling · USA

Received: 22 August 2012 / Accepted: 7 May 2013
Published online: 28 June 2013

© Springer-Verlag Berlin Heidelberg (outside the USA) 2013

Electronic supplementary material The online version of this article (doi:10.1007/s10040-013-0997-9) contains supplementary material, which is available to authorized users.

R. M. Yager (✉)
US Geological Survey,
30 Brown Rd, Ithaca, NY 14850, USA
e-mail: ryager@usgs.gov

L. N. Plummer · D. H. Doctor
US Geological Survey,
12201 Sunrise Valley Dr., Reston, VA 20192, USA

L. N. Plummer
e-mail: nplummer@usgs.gov

D. H. Doctor
e-mail: dhdoctor@usgs.gov

L. J. Kauffman
US Geological Survey,
810 Bear Tavern Rd, West Trenton, NJ 08628, USA
e-mail: lkauff@usgs.gov

D. L. Nelms
US Geological Survey,
1730 East Parham Road, Richmond, VA 23228, USA
e-mail: dlnelms@usgs.gov

P. Schlosser
Earth and Environmental Sciences,
Lamont-Doherty Earth Observatory,
139 Comer, 61 Route 9W, Palisades, NY 10964, USA
e-mail: schlosser@ldeo.columbia.edu

Introduction

Groundwater in fractured-rock aquifers flows through networks of fractures that reflect the structural history of the bedrock. Fracture networks in horizontally layered sedimentary rock typically consist of orthogonal sets of fractures that are either aligned with or cut across the bedding. Groundwater flow in fractured sedimentary rock has been simulated successfully at the kilometer scale with equivalent porous-media (EPM) models using effective hydraulic properties that represent the primary flow paths through the networks (e.g. Yager 1996; Scanlon et al. 2003; Davis and Katz 2007). Anisotropy in sedimentary-rock aquifers that results from preferential flow along bedding can be incorporated in EPM models by appropriate representation of the bedrock structure (e.g. Senior and Goode 1999; Yager et al. 2009; Yager and Ratcliffe 2010; Tiedeman et al. 2010).

 DOI 10.1007/s10040-013-0997-9

Many studies of transport of dissolved tracers through fractured-rock aquifers have focused on the dual-domain nature of these flow systems, whereby tracer concentrations in water flowing though the mobile domain are affected by diffusive exchange with concentrations in a surrounding immobile domain (Zheng and Bennett 2002). Typically, the mobile and immobile domains are assumed to represent fractures and primary pore space within the rock matrix, respectively, although it has been recognized that in some fracture networks a significant portion of the immobile domain can consist of fractures that are poorly connected to the network (Shapiro 2001). Other fracture networks can include preferential paths along intersections with fault zones or within conduits that have been enlarged through dissolution. In general, fractured-rock aquifers can be considered as multi-domain flow systems that are hydraulically connected in a hierarchical fashion. Karst aquifers can be considered as a distinct type of multiple-domain flow system in that groundwater flows through conduits that are hydraulically connected to a pervasive fracture network. These aquifers are often characterized as having quick flow through conduits and slower diffuse flow through the fracture network (e.g., Schuster and White 1971; Jones 1991). The relative proportions of conduit and diffuse flows through karst aquifers are determined by extent and degree of interconnections within the conduit network.

A primary challenge for groundwater-flow simulations of fractured-rock aquifers is the representation of multiple conductivity domains. Several computer codes have been constructed to simulate dual-domain solute transport through discrete fractures within a porous matrix that comprises a fractured-rock aquifer (e.g. Therrien and Sudicky 1996). Such codes are typically applied in site studies at the 100-m scale where a detailed geologic characterization supports the explicit specification of the spacing, orientation and extents of individual fractures within the fracture network. There are some kilometer-scale applications of discrete-fracture models where mining or proposed storage of radioactive waste has necessitated extensive mapping of the fracture network (Beaudoin et al. 2006; Blessent et al. 2011). In most kilometer-scale studies, however, it is not possible to adequately delineate fractures within the network in order to construct an accurate discrete-fracture model, and the computational requirements of such a model would render it difficult to calibrate. Groundwater flow through karst aquifers with conduit-dominated flow has been adequately simulated at the kilometer scale using EPM models with sufficient spatial resolution to delineate high permeability paths that corresponded to mapped conduits (Worthington 2009; Lindgren et al. 2011). Wu et al. (2009) simulated groundwater flow at the kilometer scale through a karst aquifer using a dual-domain, discrete-fracture model in an area in China where data from coal mining allowed a detailed delineation of conduits. In the multi-kilometer scale study presented here, the groundwater flow model was based on detailed geologic mapping and was designed to represent anisotropy in the flow system caused by bedrock structure and the influence of fault and lineament zones. Mapped faults and lineaments were represented as high conductivity zones within a porous media matrix that incorporated anisotropy along bedding planes. The model domain (912 km^2) is large enough to simulate groundwater flow on a scale that provides information relevant to groundwater managers, but is small enough to represent some of the geologic complexity that controls the flow of water and transport of environmental tracers to springs.

Environmental tracer concentrations (for example tritium, carbon-14 and chlorofluorocarbons) can provide information regarding the apparent age and age distribution of groundwater in samples from wells and springs and are useful as observations for constraining estimates of parameter values in groundwater flow models (Sanford et al. 2004; Solomon et al. 2010; Sanford 2011; Eberts et al. 2012). When using tracer data for model calibration, it is important to recognize that measured concentrations represent mixtures of waters that have traveled along different flow paths through the aquifer (Bethke and Johnson 2008). The "apparent age" associated with a tracer therefore represents a flow-weighted average age of the sampled water mixture (Weissmann et al. 2002). Consequently, measured tracer concentrations should be used as model observations rather than estimated apparent ages (Shapiro 2011). In some cases, the sampled water can be approximated as a binary mixture of two end members (for example, younger and older water). In such cases, the age and proportions of each end member can be estimated by calibrating binary-dilution models to tracer concentrations if several types of tracers are measured (Long and Putnam 2009; Eberts et al. 2012). An alternative interpretative approach involves the simulation of flow paths through the aquifer and the computation of tracer concentrations using numerical models with advective transport (Troldberg et al. 2008; Eberts et al. 2012) or solute transport models that represent dispersion (Weissmann et al. 2002; Bethke and Johnson 2008). As a consequence of the uncertainty regarding the actual tracer flow-paths and velocities, differences in simulated and observed tracer concentrations are likely to be greater than differences in simulated and observed head and flow data (Sanford 2011).

Interpretation of environmental tracer concentrations in fractured-rock aquifers can be complicated by the potential for mixing between mobile and immobile domains within the flow system, especially in settings where groundwater velocity can range over several orders of magnitude. For example, Neumann et al. (2008) discuss the possible effects of diffusive exchange between mobile and immobile domains on tritium (^3H) and helium-3 (^3He) concentrations, but their results indicate that such effects generally are most significant for waters associated with the mid-1960s bomb pulse to about 1980. Shapiro (2011) recommends incorporating as much detail as possible in representing the geologic structure that forms the framework for the flow system. The combined interpretation of environmental tracers with different atmospheric histories or those affected by different processes (for example, conservative tracers and radioactive tracers) can provide multiple lines of evidence that constrain estimates of parameter values in models of fractured-rock aquifers (Cook et al. 2005).

 DOI 10.1007/s10040-013-0997-9

Few studies have interpreted environmental tracer concentrations at the kilometer scale in fractured-rock aquifers. Shapiro (2001) used a one-dimensional (1D) transport model to estimate the rate of exchange of ^{3}H and CFC-12 between high- and low-permeability fractures in crystalline rock. Cook et al. (2005) used a discrete-fracture model to represent idealized vertical and horizontal fractures in fractured sedimentary rock in the Clare Valley Australia to simulate depth profiles of CFCs and carbon-14 concentrations and estimate groundwater age. Lindgren et al. (2011) calibrated an EPM model with advective transport to tritium concentrations in the Edwards aquifer in Texas USA and delineated recharge areas and transit times to a public-supply well. Two studies have used lumped parameter models of karst aquifers at the kilometer scale to analyze tracer concentrations. Long and Putnam (2009) analyzed CFCs and tritium concentrations in groundwater pumped from the Madison aquifer in South Dakota USA to estimate the quick and diffuse flow fractions in a bimodal age distribution within the contributing area to a well. Einsiedl et al. (2010) used tritium data in spring discharge to estimate a mean transit time (4.6 years) for diffuse flow within the Franconian aquifer in Germany.

In this study, several types of environmental tracer data were collected in spring discharge from a folded and fractured karst aquifer in the Shenandoah Valley USA in which groundwater is dominated by diffuse flow through the fracture network. Groundwater age distributions were estimated from the concentration data using a binary-dilution model (IAEA 2006; Solomon et al. 2010), and an EPM groundwater flow model with advective transport through particle tracking. The purpose of this study was to demonstrate the utility of environmental tracer data as an aid in the calibration of a numerical model of groundwater flow in folded and fractured karst, an application that has not been previously reported in the literature.

Hydrogeologic setting

Stratigraphy and structure

The watershed of Opequon Creek (referred to as the Opequon watershed herein) occupies the northwest corner of the Shenandoah Valley (Fig. 1), part of a near-contiguous karst terrain called the Great Valley that extends from the state of Alabama to New York, across a distance of approximately 1,500 km (Trapp and Horn 1997; Weary 2008). The Shenandoah Valley is underlain by both carbonate and siliciclastic rocks composed of Paleozoic marine sediments that form a northeast–southwest trending synclinorium. The carbonate rocks of the Shenandoah Valley are bound by two major fault systems, the Blue Ridge thrust on the eastern edge, and the North Mountain thrust on the western edge. The carbonate rocks are exposed along the valley flanks, with younger siliciclastic rocks forming the central portion of the valley along the axial trend of the regional fold structure (Fig. 1). The carbonate rocks comprise a sequence of more than 3,000 m of Cambrian and Ordovician platform deposits (Butts 1940) and are nearly all composed of mixed beds of limestone and dolomite (Figs. 2 and 3). The Ordovician Martinsburg Formation, a siliciclastic unit of shale and interbedded sandstone and siltstone (Dean et al. 1987, 1990), overlies the carbonate rocks. The epikarst in the Opequon watershed, the zone between carbonate bedrock and overlying unconsolidated soil and regolith, has an irregular thickness (Fig. 4) ranging from zero to 30 m (Kozar et al. 2007). Further discussion of the bedrock stratigraphy is included in the electronic supplementary material (ESM).

Faults and lineaments

The present structure of sedimentary rocks in the Shenandoah is largely a consequence of the late Paleozoic to early Mesozoic (~320–220 Ma) Alleghanian orogeny (Hatcher et al. 1989). The rock strata were folded with the axes of the anticlines and synclines oriented northeast to southwest, with two prominent sets of joints perpendicular to bedding (Jones and Deike 1981). Longitudinal joints are parallel to the strike of the northeast-trending fold axes and cross joints are perpendicular to the fold axes. Smaller cross faults that cut across bedrock strike are prevalent in the Opequon watershed (Figs. 2 and 3) and can provide pathways for fluids to rise to the surface at springs (Hobba et al. 1979; Perry et al. 1979; Kozar et al. 2007; McCoy and Kozar 2008; Nelms and Moberg 2010). A Light Detection and Ranging (LiDAR) survey of the Opequon watershed conducted by the USGS in March 2011 detected lineaments throughout the basin. These lineaments were digitized, and combined with previous lineament mapping (McCoy et al. 2005a, b). The largest, most prominent lineaments (Fig. 2) were also assumed to provide pathways for groundwater flow in the numerical model discussed further on.

Hydrology

Fractures in the Shenandoah Valley are aligned along bedding planes, joints and cleavage planes and provide a three-dimensional (3D) permeable network for a regional flow system (Kozar et al. 2007). The fracture network is intersected locally by faults that offset bedding planes and can act as barriers to horizontal flow perpendicular to the fault zone and conduits for vertical flow. Spring locations have been correlated with fault zones in carbonate rocks in the Shenandoah Valley (Harlow et al. 2005; Doctor et al. 2009). Upward flow gradients occur where cross faults and joints intersect either bedding planes or longitudinal faults (Jones and Deike 1981; McCoy and Kozar 2008).

Karst features such as sinkholes, springs, and small caves are widely distributed throughout the basin. Despite the occurrence of karst, the groundwater flow system is dominated by diffusive flow (Jones and Deike 1981; Wright 1990; Jones 1991). The perennial discharge at larger springs is artesian and the water is saturated or nearly saturated with respect to calcite, as evidenced by surficial deposits of marl, tufa and travertine that are common downstream of springs (Hubbard et al. 1985; Doctor et al. 2009). Dye-trace studies conducted up-gradient of large perennial springs often yield long travel times (weeks to months), high tracer dilutions, and

 DOI 10.1007/s10040-013-0997-9

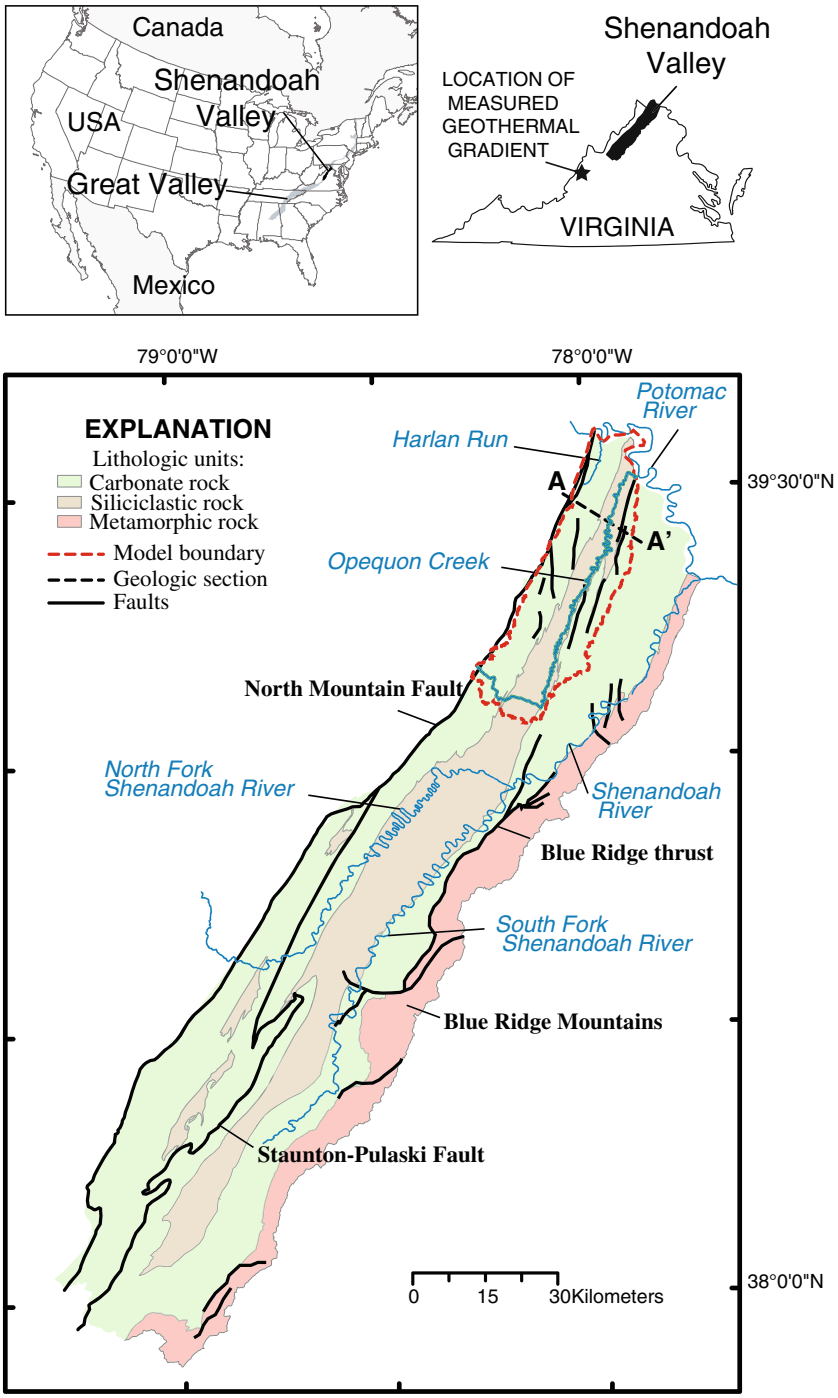

Fig. 1 Location and bedrock geology of the Shenandoah Valley

divergent flow (Jones and Deike 1981; Jones 1991, 1997; Kozar et al. 2007). A quantitative dye-trace from a sinking stream to Fay Spring (spring 6, Fig. 2) in the Opequon watershed yielded a groundwater velocity greater than 500 m day^{-1}, but with overall dye recovery of only 12 %, indicating that recent recharge mixes with a large proportion of slow-moving groundwater before emerging at the spring (Doctor et al. 2011).

Groundwater recharge

Recharge to groundwater in carbonate and siliciclastic rocks in the Shenandoah Valley occurs as infiltration from the land surface through the epikarst and weathered bedrock. Sinkholes concentrate surface runoff and convey it directly to groundwater, so recharge is unevenly distributed across the land surface. Recharge in the Shenandoah Valley has been estimated from base flow at

 DOI 10.1007/s10040-013-0997-9

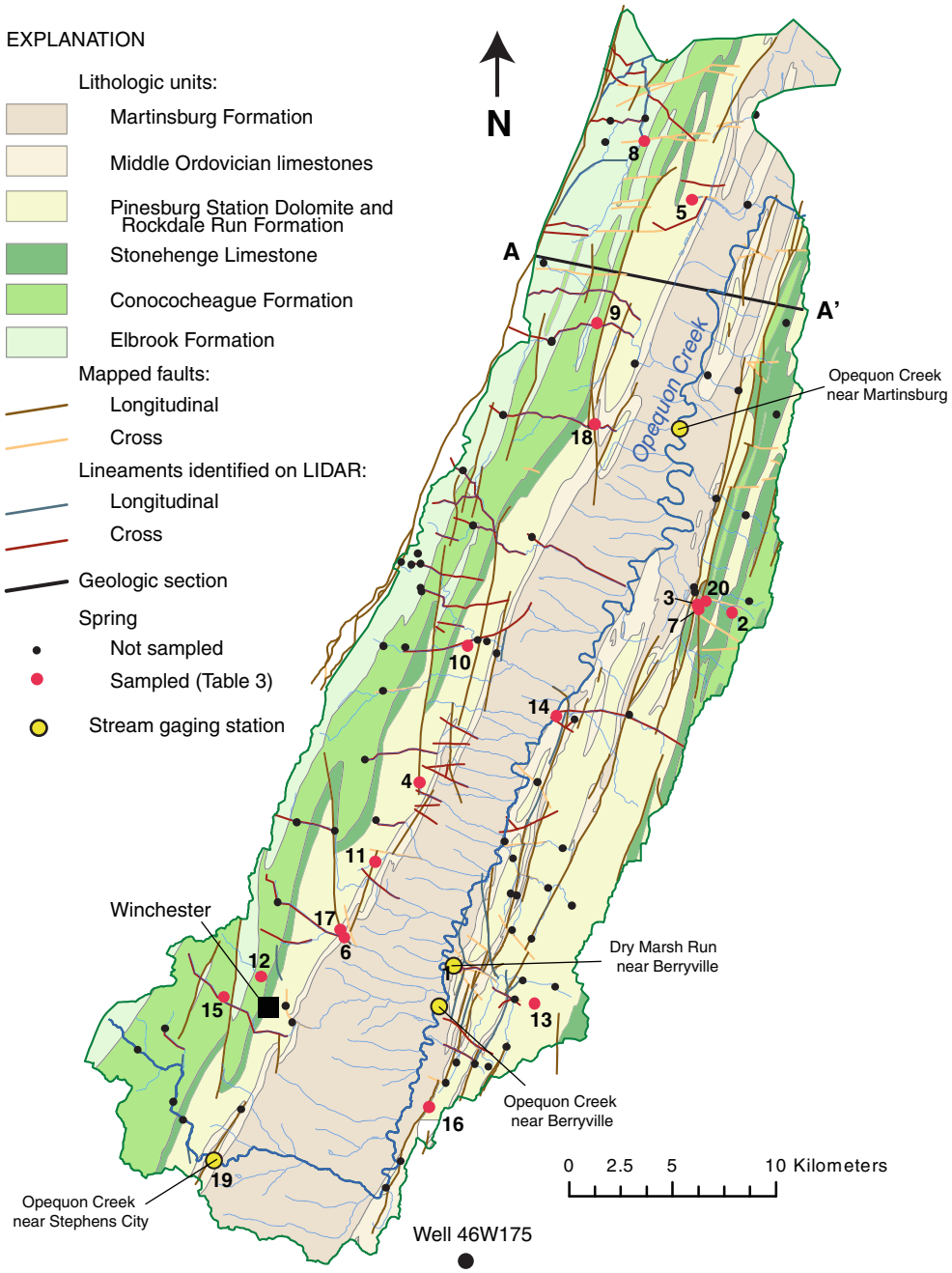

Fig. 2 Bedrock geology of the Opequon watershed showing locations of faults, lineaments and springs

20 stream flow-gaging stations (Nelms et al. 1997) and corroborated by model calibration (Kozar and Weary 2009). Base flow is linearly related to the proportions of carbonate and siliciclastic rock in the gaged watersheds; the average recharge rates for each rock type are 24.7 and 13.9 cm year^{-1}, respectively (Yager et al. 2009). In the Opequon watershed, stream flow has been measured for more than 60 years at two gaging stations and at least 5 years at two other stations (Fig. 2). The median base flow (recharge), estimated from stream-flow records, derived from both rock types in each sub-basin is presented in Table 1. Median recharge to the Opequon watershed is estimated to be 20.6 cm year^{-1} (Fig. 5a).

Groundwater discharge

Groundwater in carbonate rock in the Opequon watershed discharges to numerous springs; the median discharge of 51 springs is 1,900 m^3 day^{-1} and discharges range from 120 to 35,000 m^3 day^{-1} (Fig. 6). Many of the springs are along faults or lineaments or at stratigraphic contacts (Fig. 2). Spring discharge accounts for 60 to 90 % of stream flow (Harlow et al. 2005), and most streams draining carbonate rocks are gaining rather than losing. Total spring discharge from the Opequon watershed is estimated to be 257,000 m^3 day^{-1}. In contrast, groundwater pumped by municipal and industrial wells totaled 19,800 m^3 day^{-1} in 2001, or less than 4 % of the estimated

 DOI 10.1007/s10040-013-0997-9

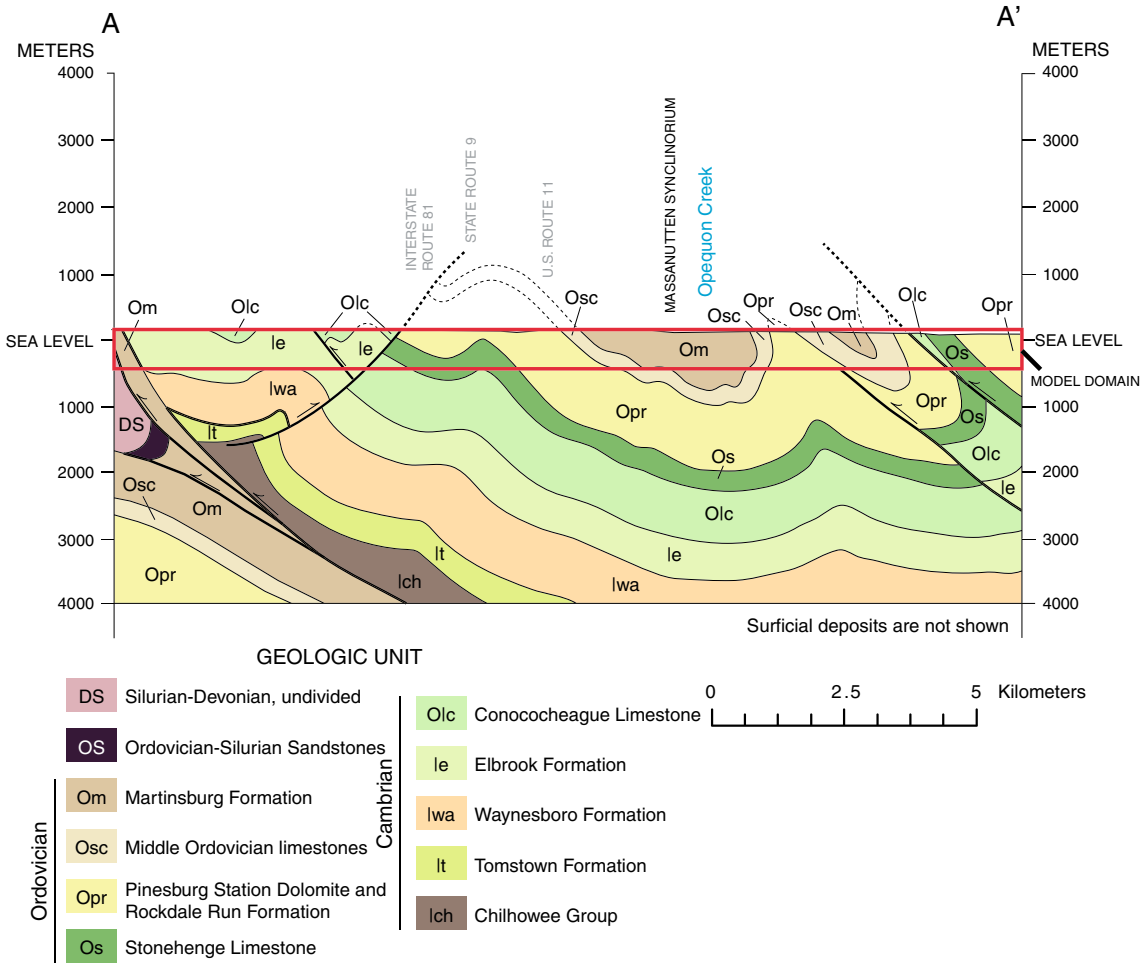

Fig. 3 Geologic section A–A' showing rock units and faults within rocks underlying the Opequon watershed

base flow. Groundwater in siliciclastic rocks discharges to stream channels that are oriented generally parallel to cross joints and perpendicular to the strike of the valley.

Circulation of groundwater through conduits and fractures in the Shenandoah Valley can exceed depths of 300 m, as evidenced by open voids intersected by a small number of deep, high-yielding wells (Cady 1936). Temperature measurements of discharge from nine springs in the Opequon watershed ranged between 10 and 16 °C, and the mean temperature (13 °C) is about 1 °C higher than the mean annual, ambient air temperature in Winchester, Virginia. A study of heat flow in folded and faulted carbonate rocks 200 km southwest of the Opequon

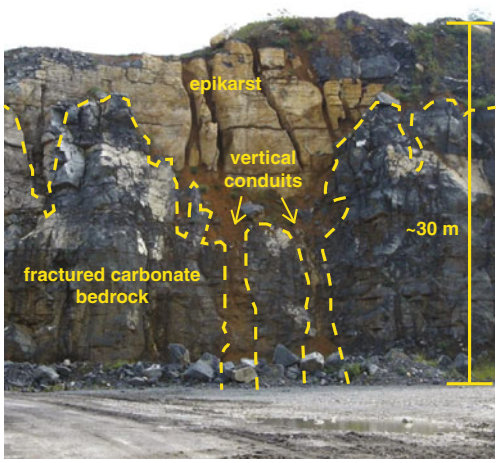

Fig. 4 Photo showing vertical conduits within the epikarst exposed in a quarry south of Martinsburg, West Virginia

Table 1 Recharge rates for carbonate and siliciclastic rocks estimated for sub-basins within the Opequon watershed

Sub-basin	Recharge rate, cm year^{-1}	
	Carbonate rock	Siliciclastic rock
Opequon Creek near Stephens City, VA	24.2	13.5
Opequon Creek near Berryville, VA	16.7	9.3
Dry Marsh Run near Berryville, VA	23.6	13.2
Opequon Creek near Martinsburg, WV	25.1	14.0
Potomac River[a]	25.1	14.0

VA Virginia, *WV* West Virginia

[a] Ungaged tributaries

DOI 10.1007/s10040-013-0997-9

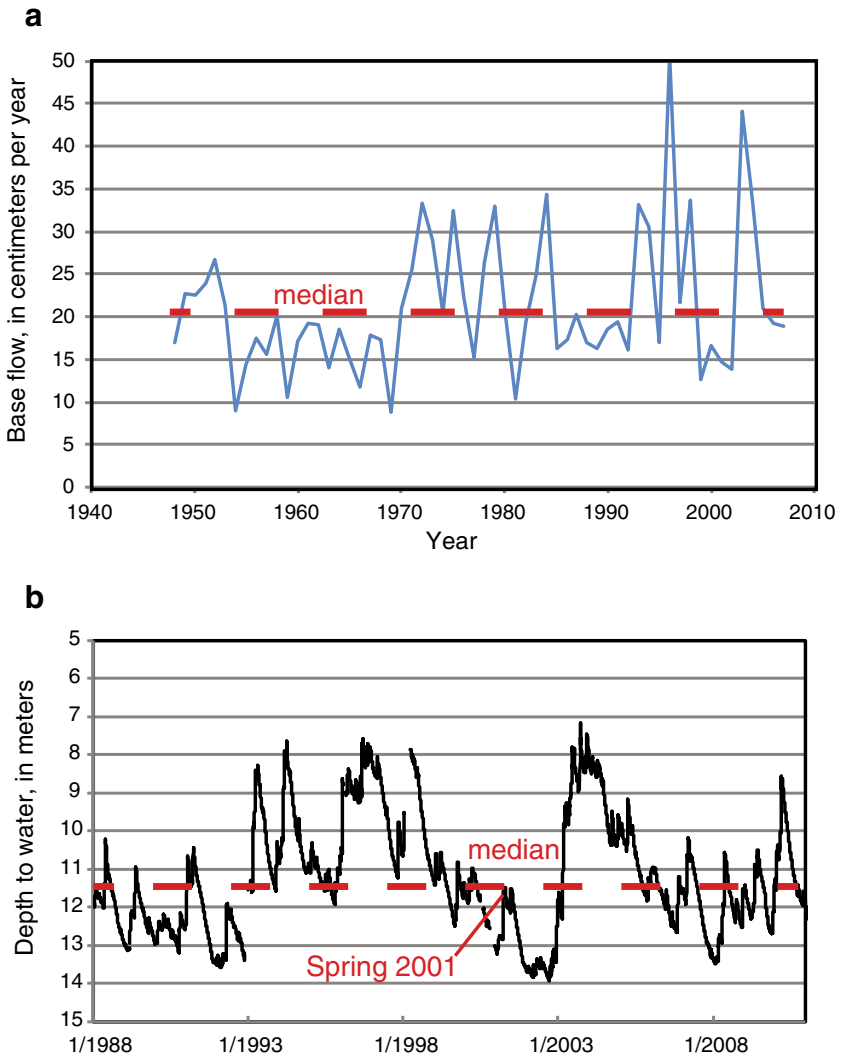

Fig. 5 Hydrographs showing **a** base flow estimated from stream flow at gage on Opequon Creek near Martinsburg, and **b** water levels in well 46W175 just east of the Opequon watershed (gage and well locations shown in Fig. 2)

watershed (Fig. 1) estimated the geothermal gradient below about 300 m depth to be 9 °C km^{-1} (Perry et al. 1979). Thus, spring temperatures elevated above ambient can be explained as an increase in temperature by 1 °C for each 100 m depth. The spring temperature data in the Opequon watershed indicates that groundwater discharged from the springs likely originated from depths of at least 100 m.

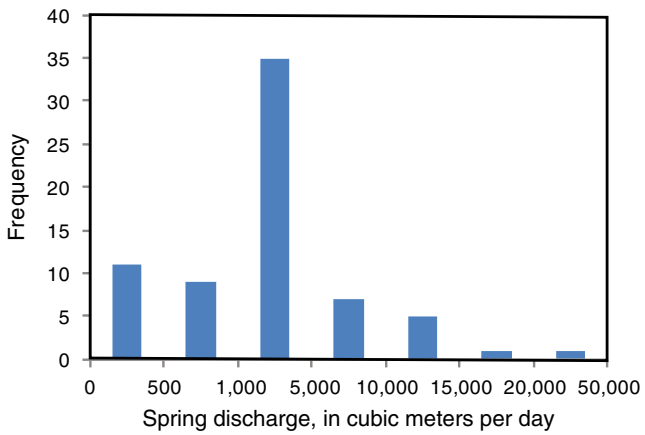

Fig. 6 Spring-discharge rates from carbonate rocks within the Opequon watershed

Hydraulic conductivity

Estimates of hydraulic conductivity for the six geologic formations underlying the Opequon watershed range from 0.3 to 3.2 m day^{-1} (see Table 1 in electronic supplementary material, ESM), based on the results of hydraulic tests conducted in West Virginia (Kozar and Weary 2009) and assuming an aquifer thickness of 40 m, the median open-interval length of wells in the Opequon watershed. The median hydraulic conductivity from hydraulic tests conducted in wells located in fault zones was 70 m day^{-1}. Estimates of transmissivity (T) for these formations are also available from the specific capacity of wells drilled in

 DOI 10.1007/s10040-013-0997-9

the Shenandoah Valley in Virginia and West Virginia. The median T values for the six formations range from 2.2 to 130 m^2 day^{-1} with a large variation in values for each formation (see Figure 1 in ESM). Median open-interval lengths and well depths were 40 and 60 m, respectively. Regression analyses indicated that the log T values are inversely related to well depth for all formations except the Martinsburg Formation, although there is wide scatter in the data.

Environmental tracers

Concentrations of environmental tracers were measured in discharge from 20 springs (Fig. 2) to obtain information on the groundwater age distribution in the Opequon watershed. Sampling periods were selected when spring discharge was mainly derived from groundwater and unaffected by storm events. The measurements include tritium (^{3}H), dissolved neon (Ne), dissolved helium-4 (^{4}He), the ^{3}He/^{4}He isotope ratio, chlorofluorocarbons (CFC-11, CFC-12, and CFC-113), and dissolved major gases, nitrogen (N_2) and argon (Ar). A discussion of sample collection and analysis is included in the ESM. Discussion of the ^{4}He analyses is also included in the ESM.

Environmental tracers and apparent groundwater age

Combinations of environmental tracers were used to identify samples of spring discharge that are mainly young (less than 60 years old) or mixtures of young and old (more than 60 years old). Dissolved major gases were used to estimate recharge temperature and excess air to correct tracer concentrations for use in age interpretation, as discussed in the ESM. The selected environmental tracer data are summarized in Table 2 along with field parameters and information on sample identification. Interpreted recharge temperature, quantities of excess air, apparent age, mixing fractions and estimated age of the young fraction are summarized in Table 3.

Tritium and chlorofluorocarbons in precipitation

Tritium data from springs in the Opequon watershed were related to a smoothed function of tritium in precipitation that was at 6-month intervals from correlation to tritium records in the US (International Atomic Energy Agency 2012). Pre-1953 values were estimated by correlations to long-term records following Michel (1989), and a constant value of 7.5 TU was assumed for the period 2006 through 2011. The tritium input function in precipitation was decay-adjusted to the year 2005, which represents the median year of sampling, for comparison with the collected data (see Figure 2 in ESM).

Atmospheric concentrations of CFCs (see Figure 2 in ESM) are available for download (US Department of Energy 2012; US Department of Commerce 2012; US Geological Survey 2012). Although CFCs can be degraded in anaerobic environments, water from most of the springs in the Opequon watershed is aerobic (Table 2). The presence of additional CFCs from non-atmospheric sources prevented the use of CFC-11 and CFC-12 concentrations in age interpretation in spring discharge in the Opequon watershed, where most CFC concentrations exceed 100 % of modern atmospheric concentrations (Table 2). In contrast, the CFC-113 concentrations are less than modern atmospheric concentrations for 12 of the 20 samples with a median value of 94 %. CFC apparent ages were calculated by relating the CFC concentration in the sample (expressed in pptv) to the historic atmospheric concentration (see IAEA 2006 for details). The average CFC-113 apparent age of the 12 valid CFC-113 samples is 16.5±3.5 years (Table 3; see Figure 3 ESM). Only spring 1 appears nearly concordant in regard to CFC apparent ages, with ages of 28.1, 20.1, and 21.6 years from CFC-11, CFC-12, and CFC-113, respectively (Table 3).

Initial tritium and tritium-^{3}He age

The apparent tritium-^{3}He (^{3}H/^{3}He) age of unmixed samples is based on the radioactive decay of tritium in precipitation to the noble gas ^{3}He. The ^{3}H/^{3}He age (τ) in years is:

$$\tau = \frac{1}{\lambda}\ln\left(1 + \frac{{}^3He_{\mathrm{tri}}}{{}^3H_{\mathrm{m}}}\right), \qquad (1)$$

where the decay constant λ=ln 2/12.32=0.05626 $year^{-1}$ (12.32 years is the half-life of tritium), ${}^3H_{\mathrm{m}}$ is the measured amount of tritium in the sample in tritium units (TU), and ${}^3He_{\mathrm{tri}}$ is the amount of tritiogenic ^{3}He in the sample produced from tritium decay, in TU. The value of ${}^3He_{\mathrm{tri}}$ can be calculated from the measured values of ^{4}He, Ne, and the ^{3}He/^{4}He isotope ratio of the sample (Schlosser et al. 1988, 1989). In an unmixed sample the apparent ^{3}H/^{3}He age is the time required for the initial tritium (${}^3H_{\mathrm{o}}={}^3H_{\mathrm{m}}+{}^3He_{\mathrm{tri}}$) to decay to the measured tritium in the sample, ${}^3H_{\mathrm{m}}$. The relatively low amounts of terrigenic ^{4}He and excess air in the samples, combined with little evidence for gas exchange following recharge, indicate that most of the apparent ages derived from the ${}^3H_{\mathrm{m}}/{}^3H_{\mathrm{o}}$ ratio in this study are reliable within 1 to 2 years. Most samples contained an excess of terrigenic ^{4}He requiring correction for terrigenic ^{3}He in age interpretation, as indicated in Table 3.

In the case of binary dilutions of young and old water, the apparent ^{3}H/^{3}He age computed with Eq. (1) is a very good approximation of the age of the young water in the mixture, if the fraction of young water is relatively large compared to that of old water and the concentration of ${}^3He_{\mathrm{tri}}$ in the old water is small. Both of these conditions are met in spring samples from the Opequon watershed (see ESM). The median apparent ^{3}H/^{3}He age of all samples computed with Eq. (1) is 4.4 years (Table 3). Figure 7a shows the decayed tritium input curve (DTIC)

 DOI 10.1007/s10040-013-0997-9

Table 2 Selected field parameters, recharge temperature, excess air, and environmental tracer concentrations measured in spring discharge in the Opequon watershed

Spring No.[a]	Spring name	Estimated discharge, $m^3 day^{-1}$ [b]	Sample date	Field water temperature, °C	Dissolved oxygen, mg L^{-1}	N_2–Ar UA[c] model recharge temperature, °C	N_2–Ar UA model excess Air, ccSTP kg^{-1} [d]	Tritium, TU[e]	δ^3He%[f]	^{4}He, ccSTP $g^{-1} \times 10^8$	Ne, ccSTP $g^{-1} \times 10^7$	CFC-11, pptv[g]	CFC-12, pptv[g]	CFC-113, pptv[g]	CFC-11, % Modern[h]	CFC-12, % Modern[h]	CFC-113, % Modern[h]
1	Afflick Spring	8,800	8/11/05	12.7	1.8	11.9	4.2	8.33	1.47	15.240	2.528	147	399	39	59	73	49
2	Bell Spring	3,700	10/16/08	12.6	6.0	13.3	2.1	6.14	3.91	5.225	2.329	5,824	47,934	538	2,321	8,787	677
3	Blue Spring	900	10/16/08	12.4	7.0	10.9	1.9	3.78	−17.78	7.022	2.329	356	651	62	142	119	78
4	Branson Spring	4,400	8/25/04	12.2	3.5	14.6	3.1	7.20	−42.21	9.753	2.201	783	659	84	312	121	106
5	Dennis Farm Spring	12,400	7/26/04	12.7	4.1	12.9	3.9	7.10	−34.26	9.608	2.469	1748	833	1,260	697	153	1,584
6	Fay Spring	3,300	8/11/03	13.0	6.5	12.7	4.3	7.83	−24.69	6.054	1.721	2,196	3,052	25,851	875	559	32,517
7	Gray Spring	2,200	9/21/09	12.1	7.6	10.4	1.2	5.30	−22.23	7.129	2.227	620	793	66	180	115	77
8	Harlan Spring	11,800	8/4/04	11.2	6.0	12.0	4.5	5.90	−26.81	9.204	2.651	3,106	737	215	1,238	135	270
9	Kilmer Spring	15,800	7/26/04	12.3	7.0	12.0	3.7	7.10	3.78	6.493	2.522	1,891	1,793	377	754	329	474
10	LeFevre Spring	6,700	5/2/06	12.0	3.7	11.8	2.4	6.70	−38.47	9.617	2.325	553	683	194	221	125	244
11	OL Payne Spring	1,400	8/24/04	12.8	2.6	11.1	3.7	8.10	−42.21	6.658	2.540	346	660	72	138	121	90
12	Old Town Spring	1,300	8/12/03	13.4	6.2	13.2	2.3	7.52	−0.44	6.275	2.385	584	612	78	233	112	98
13	Perry Spring	2,400	8/13/03	12.5	5.2	9.5	5.2	7.87	1.47	6.439	2.658	218	621	68	87	114	85
14	Priest Spring	35,200	8/4/04	11.7	3.2	11.8	5.5	5.60	−56.03	17.446	2.874	869	795	72	346	146	91
15	Robinson Spring	1,500	8/24/04	12.7	4.9	12.1	3.1	7.20	30.46	26.476	9.263	507	690	72	202	126	90
16	Salem Church Spring	1,400	8/19/04	12.7	2.6	12.0	4.8	8.14	3.12	6.191	2.635	264	585	73	105	107	92
17	Sempeles Spring	8,100	6/7/07	13.1	5.6	11.2	3.2	6.59	3.59	6.392	2.577	121	3,924	3,041	48	719	3,825
18	Snodgrass Spring	1,500	8/4/04	11.7	6.2	13.2	2.5	6.30	6.97	5.652	2.262	1,009	691	73	402	127	92
19	Springdale Spring	300	8/24/04	13.6	1.9	15.7	2.6	7.83	0.97	5.650	2.294	240	1,109	77	96	203	97
20	Tabb Spring	800	4/28/09	10.6	5.3	11.2	2.2	6.16	−0.45	5.963	2.393	167	1,297	67	67	238	84

[a] Listed in Fig. 2

[b] Historical data

[c] Unfractionated air

[d] *ccSTP* kg^{-1}, cubic centimeter at standard temperature and pressure per kilogram of water

[e] ^3H_m in TU, tritium unit. One TU=1 ^3H atom in 10^{18} H atoms=3.231 picocuries per liter (pCi L^{-1})

[f] δ^3He, in percent, = $(R/R_{air}-1)\times 100$, where $R=^3He/^4He$ ratio of sample, $R_{air}=^3He/^4He$ in air=1.384×10^{-6}

[g] *pptv* parts per trillion by volume. Computed from measured concentration in picograms per kilogram (pg kg^{-1}) using Henry's Law and corrected for excess air

[h] % Modern=$(pptv_{sample}/pptv_{air})\times 100$; pptv concentrations in modern (2005) air are 250.9 (CFC-11), 545.5 (CFC-12), 79.5 (CFC-113)

DOI 10.1007/s10040-013-0997-9

Table 3 Tritium, tritiogenic ^{3}He, initial tritium, terrigenic ^{4}He, ^{3}H/^{3}He age, fractions of young water calculated from ^{3}H and CFC-113 data, and terrigenic ^{4}He in old fraction of spring discharge in the Opequon watershed

Spring No.	Sample date	Tritiogenic ^{3}He[a], TU	Initial tritium[b], TU	Terrigenic ^{4}He[c], ccSTP $g^{-1}\times10^8$	^{3}H/^{3}He age of young fraction[d], years	^{3}H/^{3}He recharge date[e]	Age corrected for terrigenic ^{3}He?	^{3}H/^{3}H$_o$	Tritium in precipitation at ^{3}H/^{3}He recharge date[f], TU	Tritium in precipitation at recharge date decayed to sample date, TU	Binary fraction of young water from tritium[g]	Atmospheric CFC-113 at ^{3}H/^{3}He recharge date, pptv	CFC-113 apparent age[h], years	Binary fraction of young water from CFC-113[i]	Young-water fraction	Basis for young-water fraction	Old-water fraction	Terrigenic ^{4}He in old-water fraction[j], ccSTP $g^{-1}\times10^8$	Age of old-water fraction[k], years
1	8/11/05	16.93	25.3	9.04	19.9	1985.7	Yes	0.330	29.8	9.8	0.85	44.8	21.6	0.87	0.87	CFC-113	0.13	69.68	2489
2	10/16/08	1.72	7.9	-	4.4	2004.4	Yes	0.781	8.0	6.3	0.98	79.3	-	-	0.98	^{3}H	0.02	-	-
3	10/16/08	1.33	5.1	1.43	5.4	2003.4	Yes	0.740	8.4	6.2	0.61	80.1	20.8	0.78	0.78	CFC-113	0.22	6.38	228
4	8/25/04	1.64	8.8	4.40	3.7	2001.1	Yes	0.815	10.0	8.2	0.88	82.1	11.7	1.02	0.88	^{3}H	0.12	36.82	1315
5	7/26/04	1.56	8.7	3.55	3.6	2001.0	Yes	0.820	10.0	8.2	0.87	82.1	-	-	0.87	^{3}H	0.13	26.41	943
6	8/11/03	3.88	11.7	2.15	7.2	1996.4	Yes	0.669	14.8	9.9	0.79	84.4	-	-	0.79	^{3}H	0.21	10.19	364
7	9/21/09	2.23	7.5	1.88	6.3	2003.4	Yes	0.704	8.4	5.9	0.90	80.1	21.7	0.77	0.77	CFC-113	0.23	8.05	287
8	8/4/04	1.21	7.1	2.65	3.4	2001.2	Yes	0.830	10.0	8.3	0.71	82.1	-	-	0.71	^{3}H	0.29	9.23	329
9	7/26/04	3.46	10.6	0.30	7.1	1997.4	Yes	0.672	15.2	10.2	0.70	84.2	-	-	0.70	^{3}H	0.30	1.00	36
10	5/2/06	1.78	8.5	4.00	4.2	2002.1	Yes	0.790	10.1	8.0	0.84	81.5	-	-	0.84	^{3}H	0.16	24.48	874
11	8/24/04	-[l]	-	0.44	-	-	-	-	-	-	-	79.3[n]	15.1	0.90	0.90	CFC-113	0.10	4.58	164
12	8/12/03	2.65	10.2	0.44	5.4	1998.2	Yes	0.739	13.3	9.9	0.76	83.9	13.1	0.93	0.93	CFC-113	0.07	6.27	224
13	8/13/03	0.96	8.8	-	2.1	2001.5	No	0.891	10.2	9.1	0.87	81.7	14.6	0.83	0.83	CFC-113	0.17	-	-
14	8/4/04	2.25	7.8	10.25	6.1	1998.5	Yes	0.713	14.3	10.2	0.55	83.5	15.1	0.87	0.87	CFC-113	0.13	75.93	2712
15	8/24/04	-[m]	-	-	-	-	-	-	-	-	-	82.2	15.1	0.87	0.87	CFC-113	0.13	-	-
16	8/19/04	1.46	9.6	-	3.0	2001.6	No	0.848	10.2	8.6	0.95	81.7	15.1	0.89	0.89	CFC-113	0.11	-	-
17	6/7/07	1.71	8.3	-	4.1	2003.3	No	0.500	8.4	6.7	0.99	80.1	-	-	0.99	^{3}H	0.01	-	-
18	8/4/04	3.57	9.9	0.17	8.0	1996.5	Yes	0.638	14.8	9.5	0.67	84.4	15.1	0.87	0.87	CFC-113	0.13	1.30	46
19	8/24/04	-[l]	-	-	-	-	-	-	-	-	-	79.3[n]	14.1	0.97	0.97	CFC-113	0.03	-	-
20	4/28/09	1.23	7.4	0.18	3.3	2006.0	Yes	0.834	7.5	6.2	0.99	78.6	20.8	0.85	0.85	CFC-113	0.15	1.17	42

[a] Tritiogenic ^3He, $^3He_{tri}$, i.e., the amount of ^3He in sample derived from radioactive decay of ^3H, in tritium units, TU

[b] Initial tritium, $^3H_o = {}^3H_m + {}^3H_{tri}$

[c] See Equation 2 in ESM; Values denoted "-" are approximately zero within uncertainties of the calculation

[d] Eq. (1)

[e] Sample date from Table 3 minus $^3H/^3He$ age

[f] From tritium in precipitation input function (see Figure 2 in ESM)

[g] Eq. (2)

[h] Values denoted "-" are samples that contain CFC-113 from non-atmospheric sources

[i] Eq. (3)

[j] See Equation 3 in ESM

[k] See Equation 5 in ESM using the model-derived ^{4}He accumulation rate of 2.8×10^{-10} ccSTP g^{-1} $year^{-1}$

[l] Calculated $^3He_{tri}$ is small

[m] Air leak in copper sample tube

[n] ^{3}H/^{3}He age of zero assumed in CFC-113 binary mixing calculations

DOI 10.1007/s10040-013-0997-9

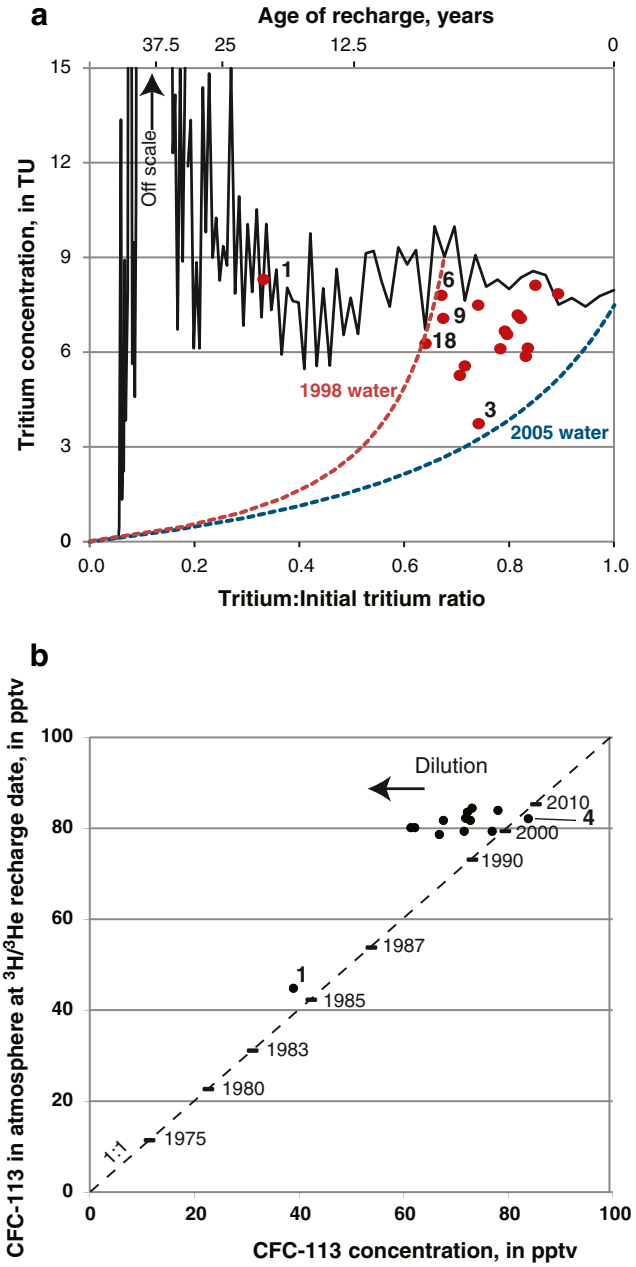

Fig. 7 Graphs showing **a** Tritium measured in spring discharge (^3H_m) and tritium-in-precipitation decayed to the year 2005, as a function of sample age and as a function of the tritium/initial tritium ratio ($^3H_m/^3H_o$), and **b** CFC-113 measured in spring discharge and atmospheric CFC-113 at recharge date, as estimated from $^3H/^3He$ age. The *upper horizontal axis* (**a**) is the sample age relative to the year 2005 an unmixed (piston flow) sample. The *curved lines* (**a**) represent dilution of water recharged in 2005 and 1998 by old water, the fraction of which increases along the mixing line as it approaches the origin. The old water fraction is assumed to contain 2 TU of $^3H_{tri}$. Evidence for dilution with old water also is seen in the CFC-113 data (**b**) as most samples plot to the left of the piston flow line, toward CFC-113 concentrations lower than expected according to the $^3H/^3He$ age

as a function of the $^3H_m/^3H_o$ ratio for unmixed (piston flow) samples. The upper horizontal axis indicates the initial recharge date for unmixed samples. In binary dilutions the $^3H_m/^3H_o$ ratio varies along a curve from 0 (old) to 1.0 (modern), as a function of age. Two binary-dilution mixing lines are shown in Fig. 7a: one for dilution of water recharged in 2005 (zero age) and one for dilution of water recharged in the year 1998 (7 year-old tritium-bearing water). Most of the samples plot below the DTIC and between these two mixing lines, and appear to be mixtures of young, tritium-bearing water with ages between 0 and 7 years and older water that contains little or no tritium. The sample from spring 1 appears to be unmixed, however, and plots along the DTIC with a $^3H/^3He$ age of about 20 years.

A second graph (Fig. 7b) compares CFC-113 concentrations (in pptv) in the spring samples to atmospheric CFC-113 concentrations corresponding to the apparent $^3H/^3He$ recharge date of each sample. Unmixed samples not affected by dilution (piston flow) would plot along the 1:1 line. Spring 1 has the oldest recharge date (about 1985) with the lowest measured CFC-113 concentration and only a small amount of dilution with old water (Fig. 7b). Most of the samples have recharge dates more recent than the year 2000 and plot to the left of the piston-flow line, indicating that they have been diluted with old water. The apparent ages from CFC-113 concentrations and the $^3H/^3He$ ratio are compared (see Figure 3 in ESM) for samples with valid CFC-113 concentrations (those samples with less than 100 % modern CFC-113) and those with valid apparent $^3H/^3He$ ages (Tables 2 and 3). The apparent CFC-113 ages are all older than the apparent $^3H/^3He$ ages (Table 3), suggesting that the spring discharges can be approximated as binary mixtures of young and old water.

Mixing fractions of young and old water

If mixtures of young and old (tracer-free) water are approximated with a binary-dilution model and the $^3He_{tri}$ concentration of old water is neglected (see ESM) the mixing fractions of young and old water (f_{young} and f_{old}) can be estimated using the apparent $^3H/^3He$ age (and date of recharge) of young water in the sample (Eq. 1). The fraction of young water based on tritium ($f_{young(^3H)}$) is calculated from the initial tritium in the sample (^3H_o) and the amount of tritium in precipitation at the time of recharge ($^3H_{precip}$), based on the apparent $^3H/^3He$ age and the DTIC (see Figure 2 ESM), as:

$$f_{young(^3H)} = \frac{^3H_o}{^3H_{precip}} \quad . \tag{2}$$

Although ^3H_o can be measured within about ±0.3 TU, the amount of ^3H in precipitation at time of recharge probably is not known better than about ±10 % and can vary widely with both seasonal and individual precipitation events.

For the 12 samples that contain valid CFC-113 concentrations (Table 3), the fraction of young water ($f_{young(CFC\text{-}113)}$) was calculated using the amount of CFC-113 in the atmosphere at the time of recharge ($CFC\text{-}113_{atm}$), where the recharge date was defined by the apparent $^3H/^3He$ age (Eq. 1):

$$f_{young(CFC-113)} = \frac{CFC-113}{CFC-113_{atm}} . \tag{3}$$

DOI 10.1007/s10040-013-0997-9

The accuracy of the measured CFC-113 concentrations is about 2 % and the atmospheric concentrations of CFC-113 in North America air are known within a similar precision, although some samples could contain small amounts of non-atmospheric CFC-113 (making the apparent age appear younger).

The fractions of young water for 10 samples computed from both the ^{3}H and CFC-113 data (Table 3) are compared in Fig. 8. The average young-water fraction obtained from the ^{3}H data is 0.82±0.13 (17 samples), while the average young-water fraction obtained from the CFC-113 data is 0.88±0.07 (13 samples). The fractions of young water estimated from the ^{3}H data for three springs (3, 14 and 21) are lower than those estimated from the CFC-113 data (Fig. 8). This difference could be due to either excess CFC-113 in the samples or over-estimation of the amount of tritium in precipitation at time of recharge. The error bars shown in Fig. 8 were computed accounting for a 10 % uncertainty in tritium in precipitation at time of recharge, and 2 % uncertainty in CFC-113 measured concentration. Uncertainty in the measured tritium and in the atmospheric mixing ratio of CFC-113 were judged smaller and not included in the error analysis. Given the uncertainty in reconstructing the tritium concentration in precipitation compared to uncertainty in CFC-113 concentrations, the fractions of young water computed from the CFC-113 data are assumed to be more accurate than those based on the ^{3}H data. The fractions of young water computed from ^{3}H data, however, were used for the eight springs for which the CFC-113 concentrations were not valid (Table 3).

Overall, the fraction of young water for the 20 springs in the Opequon watershed ranges from 0.70 to 0.99 with an average value of 0.86±0.08. The error associated with neglecting the $^{3}He_{\text{tri-old}}$ concentration in the binary-dilution model is small, as discussed in the ESM. Binary-dilution model estimates of mixing fractions computed with CFC-113 data are more reliable than those based on ^{3}H data because the atmospheric mixing ratio of CFC-113 has been nearly constant for the past 15 years, but could contain an error less than 5 % for young-water fractions more than 0.4 (see Figure 4a in ESM). Estimates of mixing fractions based on ^{3}H data could be over-estimated by less than 5 % for mixtures that contain young-water fractions more than 0.6 and 2 TU of $^{3}\text{He}_{\text{tri-old}}$ (see Figure 4b in ESM). If, in the extreme case, the old water contains 5 TU of $^{3}He_{\text{tri-old}}$, the approximation is still very good for mixtures that contain young-water fractions greater than 0.8, which is the case for nearly all the computed mixtures (Table 3).

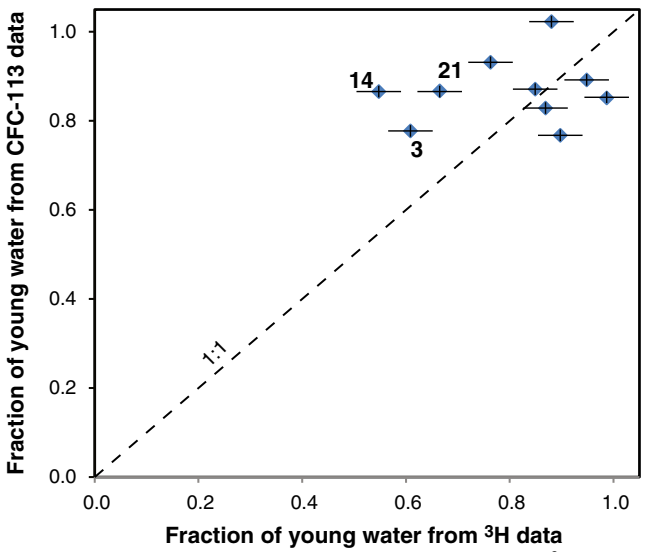

Fig. 8 Comparison of fractions of young water based on ^{3}H (Eq. 2) and on CFC-113 (Eq. 3). *Error bars* for estimated fractions based on ^{3}H are shown

Numerical model

Groundwater flow in the Opequon watershed was simulated as steady-state with a 3D finite-difference model using MODFLOW (Harbaugh et al. 2000) to represent a period in April 2001 when a long-term well hydrograph indicates that water levels were near 12-year median values (Fig. 5b). The model represents a 500-m thickness of carbonate and siliciclastic rock and overlying epikarst. The geometry of the flow model is based on a 3D geologic model that contains six bedrock units that are intersected by mapped faults and lineaments.

Model design

The model domain covers an area of 915 km^2 and includes the watersheds of Opequon Creek and Harlan Run, with the exception of a 50-km^2 area in the Opequon watershed west of the model domain underlain predominantly by siliciclastic rock (Fig. 9). The model domain is discretized using a regular grid of 100-m square cells that are small enough to resolve fault zones in the carbonate rock and perennial stream channels within the siliciclastic rock. The grid is oriented N 23° E, parallel to the generalized strike of the sedimentary rocks. The top surface of the model corresponds to land surface based on a 10-m digital elevation model (DEM) and the bottom surface is specified as 500 m below land surface. The rock mass is divided into 6 layers: two upper layers that are each 25-m thick and four lower layers of increasing thickness from 50 to 200 m (Fig. 10b). The resulting grid contains 542,334 active cells. The top model layer represents either siliciclastic rock, or the epikarst in areas underlain by carbonate rocks.

Model boundary conditions

The lateral boundaries of the model domain generally coincide with watershed boundaries and are, therefore, assumed to be no-flow. The generalized water-table surface of the northern part of the Shenandoah Valley supports the assumption that the groundwater and watershed divides overlap, although the position of the groundwater divide probably moves seasonally in response to changes in

 DOI 10.1007/s10040-013-0997-9

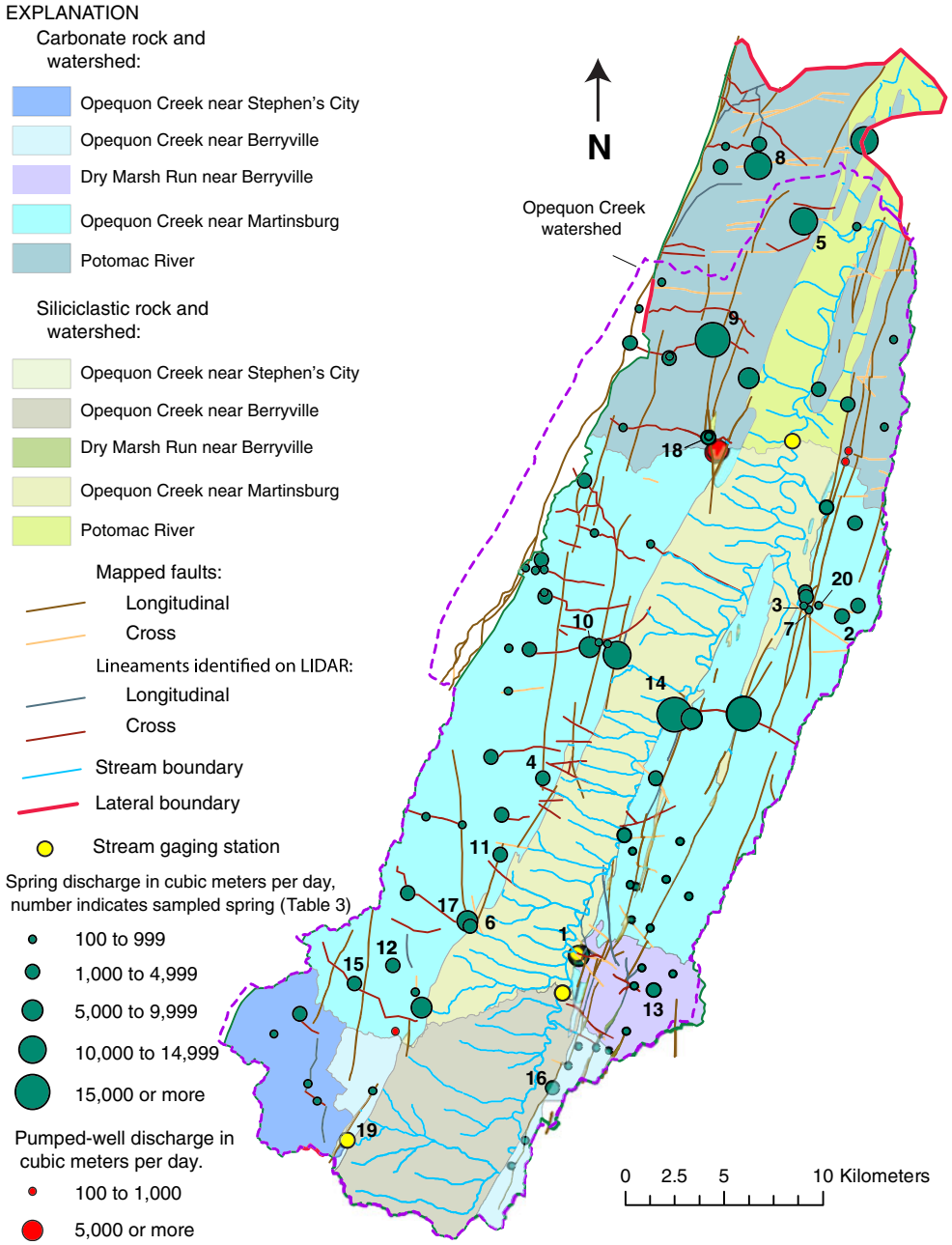

Fig. 9 Model domain and boundaries showing distribution of carbonate and siliciclastic rocks within gaged sub-basins within the Opequon watershed

recharge. The northern boundary of the model domain represents discharge to the Potomac River through seepage faces using a head-dependent flow boundary (drain cells) assigned an elevation of 110 m (Fig. 9). The hydraulic conductivity value that limits discharge through this boundary was estimated through model calibration. Underflow into the model domain from the portion of the Opequon watershed excluded from the domain is represented as a specified flow along the western model boundary and was estimated through model calibration. Underflow out of the model domain toward a pumping center near a quarry operation is represented as a specified flow along the southern model boundary based on measured pumping rates.

The top model boundary represents recharge as a specified flow using the recharge rates for carbonate and siliciclastic rocks presented earlier for each sub-basin in Table 1. Total recharge to the model domain is 509,000 m^3 day^{-1}, based on median recharge to the Opequon watershed (20.6 cm^{-1} year). The bottom model boundary represents vertical flow into and out of the model domain. The depth of the sedimentary basin beneath the Opequon watershed exceeds 4 km (Fig. 3) and it was not practical to represent the entire bedrock thickness. A regional groundwater-flow model of the Shenandoah Valley of Yager et al. (2009) indicates downward flow beneath recharge areas within the Opequon watershed and upward flow beneath tributary stream channels. This pattern of flow

 DOI 10.1007/s10040-013-0997-9

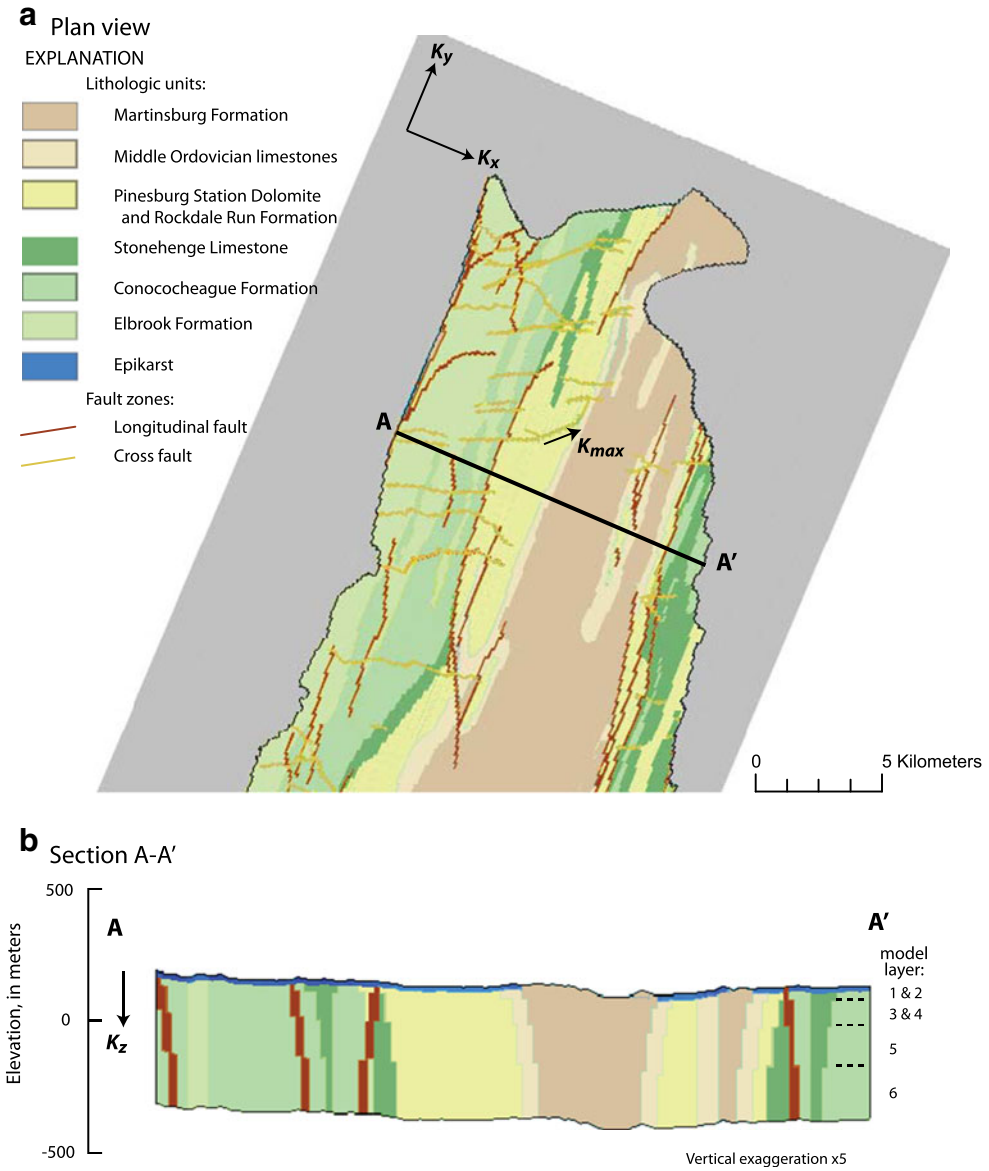

Fig. 10 Representation of rock units and fault zones in model of Opequon watershed. **a** Plan view, and **b** section *A–A′*.

was represented in the Opequon model by specifying downward flow through the bottom model boundary within carbonate rock and upward flow along fault zones. The downward and upward flow rates were estimated during model calibration.

Groundwater discharge to 92 springs in carbonate rocks and perennial stream channels in siliciclastic rocks is represented by head-dependent flow boundaries (drain cells). The springs are assumed to discharge water from the upper 125 m of the carbonate rocks, based on measured temperatures of spring water presented earlier, and are represented by a stack of three drain cells in model layers 2–4 (Fig. 9). Each spring elevation was assumed to lie 2 m below the simulated water table in the model cell that contained the spring. Streambed hydraulic-conductivity values (K_{str}) that limit discharge to springs and streams were estimated through model calibration. Pumping from five municipal and industrial wells (19,800 m^3 day^{-1}) is represented by specified flow boundaries.

Hydraulic conductivity

Hydraulic conductivity in fractured sedimentary rock can be represented by a 3D hydraulic conductivity tensor (herein referred to as the conductivity tensor) that is oriented with the directions of maximum and medium hydraulic conductivity parallel to the strike and dip of bedding, respectively, and the minimum hydraulic conductivity direction perpendicular to bedding (e.g., Yager et al. 2009). The conductivity tensors defined by the MODFLOW grid that represent the Opequon watershed vary two-dimensionally in the horizontal direction, but are oriented vertically. As a result, the representation of the actual bedrock structure in the Opequon watershed in the model is approximate.

 DOI 10.1007/s10040-013-0997-9

Six rock units and the epikarst overlying carbonate rocks were assigned separate values of hydraulic conductivity that were estimated through model calibration (Table 4; Fig. 10). Bedding in the siliciclastic Martinsburg Formation that underlies the center of the watershed was assumed to be horizontal, while bedding in the five carbonate units located along the east and west flanks of the watershed was assumed to be vertical. This approximation is justified by the generally large dip of carbonate rock units in the study area (Fig. 3). The direction of maximum hydraulic conductivity (K_{max}) in all six rock units was oriented parallel to the generalized strike of the valley (N 23° E) along columns of the model grid (*y*-direction). In the Martinsburg Formation the direction of medium hydraulic conductivity was specified as perpendicular to strike (along model rows, *x*-direction), so the K_{max}:K_{med} anisotropy was represented as horizontal anisotropy (K_y:K_x). The direction of minimum hydraulic conductivity in the Martinsburg Formation (perpendicular to bedding) was vertical (*z*-direction), so the K_{max}:K_{min} anisotropy was represented as vertical anisotropy (K_y:K_z).

The direction of medium hydraulic conductivity in the six carbonate units was specified as vertical (parallel to the dip of the bedding), and the K_{max}:K_{med} anisotropy was represented as vertical anisotropy (K_y:K_z). The direction of minimum hydraulic conductivity in the carbonate units was horizontal, so the K_{max}:K_{min} anisotropy was represented as horizontal anisotropy (K_y:K_x). The direction of maximum hydraulic conductivity in the epikarst was assumed to be vertical and the magnitudes of K_{med} and K_{min} were assumed to differ by a factor of four, so K_z:K_y= $4 \cdot K_z$:K_x. The following power function was applied to decrease K_{max} in the carbonate units, fault zones and lineaments with increasing depth below land surface (as indicated by specific capacity data):

$$K_{depth} = K_{max} 10^{-\lambda d}, \quad (4)$$

where K_{depth} is the maximum hydraulic conductivity [L T^{-1}] at depth d [L] below a threshold depth D and λ is a decay coefficient [L^{-1}]. The threshold depth was assumed to be 150 m, which is greater than the median well depth and corresponded to the bottom of layer 4. The λ value was estimated through model calibration.

Mapped faults and lineaments generally intersect the carbonate rocks and were classified as longitudinal faults (sub-parallel to bedding strike) or cross faults (perpendicular to bedding strike). Fault zones that correspond to the mapped faults and lineaments are assumed to be 100 m wide and oriented vertically. The conductivity tensors defined for the fault zones using the Model-Layer Variable-Direction Horizontal Anisotropy (LVDA) package in MODFLOW (Anderman et al. 2002) are oriented such that the directions of K_{max} are parallel to the mapped strikes. The direction of medium hydraulic conductivity was specified as vertical and the magnitudes of K_{max} and K_{med} were assumed equal, so K_{max}:K_{med}=1. The directions of K_{min} were horizontal and perpendicular to the mapped strikes.

Advective transport

Groundwater flow paths and advective travel times were calculated using MODPATH (Pollock 1994) to delineate areas contributing recharge to springs and compute distributions of travel times of recharge through the model domain to springs. Separate porosity values (n) assigned to the epikarst, siliciclastic rocks, carbonate rocks and the fault zones were estimated through model calibration. A power function similar to Eq. (4) was applied to decrease the porosity values with increasing depth in all units with a decay coefficient λ and a threshold depth of 150 m.

Particles were tracked backward from the faces of drain cells that represented spring discharge to inflow boundaries within the model domain. Travel time within the drain cell was assumed to be negligible. The number of particles assigned to each drain-cell face was based on the proportion of the total simulated spring discharge that flowed through the face, so that each particle represented approximately the same quantity of flow. About 2,000 particles were tracked from each spring, but the actual number of particles per face (np_{face}) was varied so the starting positions could be configured as a square array on each cell face. The fraction of the total simulated discharge associated with the *pth* particle (X_p) was calculated as:

$$X_p = \frac{Inflow_{face}/np_{face}}{Inflow_{total}}, \quad (5)$$

where $Inflow_{face}$ is the volume of flow through the cell face, and $Inflow_{total}$ is the total inflow into the drain cells representing the spring.

The program MODPATH-OBS (Hanson et al. 2012) was used to compute concentrations of tritium, CFC-113 and ^{4}He in spring discharge. The concentration-histories of tritium and CFC-113 were specified in recharge and tracked along particle flow paths to springs using travel times computed by MODPATH. The average tracer concentration for all particles that discharge at drain cells representing a spring was computed as a flow-weighted average concentration in the simulated discharge. Upward flow along fault zones through the bottom model boundary was assumed to represent water older than 60 years and was assigned zero concentrations of tritium and CFC-113. Tritium and CFC-113 concentrations derived from recharge were, therefore, diluted by mixing with particles that originated from the bottom model boundary.

Simulated concentrations of tritium ($C_{tritium}$) were decreased along flow paths to account for radioactive decay of tritium to ^{3}He with an equation describing first-order decay:

$$C_{tritium} = \sum_{1}^{np} X_p \left(RC_{rt_p} e^{-kt_p} \right) \quad (6)$$

where np is the number of particles associated with the drain cells representing a spring, RC is the tritium concentration in recharge at the recharge time (rt_p) (calculated as the sample time minus the travel time) of

 DOI 10.1007/s10040-013-0997-9

Table 4 Parameter values estimated and specified in nonlinear regression

Parameter	Value	Coefficient of variation, percent		
		All observations	Head and flow observations	Effective hydraulic conductivity[a]
Maximum hydraulic conductivity[b], m day^{-1}				
Martinsburg Formation	0.32[c]	9.6	20	0.23
Middle Ordovician limestones	18.4[c]	5.1	42	4.3
Pinesburg Station Dolomite/Rockdale Run Formation	16.8[c]	3.1	35	3.7
Stonehenge Limestone	16.8	–	–	3.7
Conococheague Formation	2.3[c]	11	53	0.77
Elbrook Formation	19.9[c]	4	22	4.5
Epikarst	1	–	–	–
Cross faults	19.2[c]	3.8	21	8.6
Longitudinal faults	2.8[c]	17	36	1.5
Depth coefficient, day^{-1}	0.002	–	–	–
Anisotropy ratios—maximum:medium[d]				
Martinsburg Formation	2	–		
Middle Ordovician limestones	2.6[c]	14	41	
Pinesburg Station Dolomite/Rockdale Run Formation	2.6	–		
Stonehenge Limestone	2.6	–		
Conococheague Formation	2.6	–		
Elbrook Formation	2.6	–		
Epikarst	5	–		
Cross faults	1	–		
Longitudinal faults	1	–		
Anisotropy ratios—maximum:minimum[e]				
Martinsburg Formation	10	–		
Middle Ordovician limestones	18[c]	5.2	63	
Pinesburg Station Dolomite/Rockdale Run Formation	21[c]	3.9	33	
Stonehenge Limestone	21	–		
Conococheague Formation	9[c]	7.8	31	
Elbrook Formation	20	–		
Epikarst	20	–		
Cross faults	5	–		
Longitudinal faults	5	–		
Streambed hydraulic conductivity, m/day				
Streams	0.05[c]	8.3	254[j]	
Springs[f]: large (>350 m^3 day^{-1})	0.12[c]	1.5	7.3	
Springs[f]: small (<350 m^3 day^{-1})	0.01[c]	29	38	
Potomac River[g]	0.03[c]	2.9	18	
Specified flows, m^{3}day^{-1}				
Western boundary	14,400	–		
Bottom boundary: upward[h]	98,800[c]	1.2	75	
Bottom boundary: downward[i]	98,800[c]	6.7	11	
Porosity, percent				
Epikarst	1.5[c]	8.5		
Martinsburg Formation	1	–		
Carbonate rocks	0.86[c]	4.5		
Faults	0.38[c]	18		
Depth coefficient, day^{-1}	0.005	–		
^{4}He				
Concentration, ccSTP g^{-1}	4.9E-07[c]	3.2		
Accumulation rate, ccSTP g^{-1} year^{-1}	2.8E-10[c]	2.2		

[a] $K_e=(K_{max}K_{min})^{1/2}$

[b] Martinsburg Formation and carbonate rocks: $K_{y,}$; Epikarst: K_z; faults: K_{max}

[c] Estimated parameter values

[d] Martinsburg Formation: K_y:K_x; carbonate rocks: K_y:K_z; Epikarst: K_z:K_y; faults: K_{max}:K_z

[e] Martinsburg Formation: K_y:K_z; carbonate rocks: K_y:$K_{x,}$ Epikarst: K_z:$K_{x,}$ faults: K_{max}:K_{min}

[f] Hydraulic conductivity assumes 5 and 2-m diameter for large and small springs, respectively

[g] Hydraulic conductivity of seepage face

[h] Fault zones

[i] Carbonate rock

[j] Highly uncertain estimate

the pth particle, k is the decay rate, and t_p is the travel time of the pth particle. The ^{3}He concentration associated with each particle was calculated from the amount of tritium decay along the particle's flow path.

 DOI 10.1007/s10040-013-0997-9

The simulated ^{4}He concentration along each flow path ($C_{\text{He-4}}$) was assumed to accumulate following an equation that describes zero-order growth:

$$C_{\text{He-4}} = \sum_{1}^{np} X_{\text{p}}\left(RC_{\text{rt}_{\text{p}}} + k_{\text{t}_{\text{p}}}\right) \quad (7)$$

where k is the accumulation rate. The initial value of $C_{\text{He-4}}$ at the bottom model boundary and the accumulation rate were estimated through model calibration.

Model calibration

The groundwater flow model was calibrated to estimate model parameters through nonlinear regression with UCODE (Poeter and Hill 1998; Poeter et al. 2005) using measured groundwater levels in 485 wells and discharges at 2 streamflow-gaging stations and 51 springs in the Opequon watershed. The regression also included 60 concentration observations derived from environmental tracer data collected at 20 springs. The estimated parameters included K_{max} of six bedrock units, epikarst and fault zones, four anisotropy ratios (K_{max}:K_{med} and K_{max}:K_{min}) of carbonate rocks, and four K_{str} values of stream and spring boundaries (Table 4). Four porosity values of carbonate rocks and fault zones, and the two values associated with accumulation of ^{4}He (Equation 5 in ESM) were also estimated by regression. A discussion of the observations used in model calibration and figures showing the spatial distribution of residuals (observed minus simulated values) are included in the ESM (see Figure 6 in ESM).

Estimated parameters

A total of 40 parameters are defined in the groundwater-flow model and 21 were optimized through nonlinear regression (Table 4). The remainder were specified or estimated through regressions that decreased model error, but did not converge to optimum values. All of the optimized parameters are well-estimated and the coefficients of variation for most estimates are less than 10 %. Seven values of K_{max} were estimated for the bedrock units and fault zones. The K_{max} values were lowest (0.32 m day^{-1}) for the Martinsburg Formation and ranged from 2.3 to 19.9 m day^{-1}for carbonate rocks. The K_{max} values for the bedrock units in the bottom two model layers (70 % of the model domain) were reduced by factors of 3 and 6, respectively, using Eq. (4) with a specified depth coefficient (λ) that was estimated by trial and error. The K_{max} values for cross and longitudinal fault zones were 19.2 and 2.8 m day^{-1}, respectively. Data are not available to either support or contradict the difference in these model-derived estimates for the K_{max} values of fault zones. Field observations indicate that zones of rising groundwater occur more frequently along cross-strike features, however, as indicated by the presence of marl in stream channels parallel to cross-strike faults.

Optimum estimates of four anisotropy ratios were obtained through regression for the carbonate rocks (Table 4) including the K_{max}:K_{med} anisotropy (strike-parallel to dip-parallel conductivity) and three K_{max}:K_{min} anisotropy values (strike-parallel to cross-bedding conductivity). The K_{max}:K_{min} anisotropy ratios ranged from 9:1 for the Conococheague Formation to about 20:1 for the other carbonate units, which is comparable to the ratio obtained through calibration of a groundwater-flow model of the Shenandoah Valley (17:1) by Yager et al. (2009). Other anisotropy ratios in the Opequon model were specified. The K_{max}:K_{min} anisotropy values for the epikarst (K_z:K_{xy}) and fault zones (strike-parallel to strike-perpendicular conductivity) were 20:1 and 5:1, respectively. The K_{max}:K_{med} (strike-parallel to strike-perpendicular conductivity) and K_{max}:K_{min} (strike-parallel to cross-bedding conductivity) anisotropy ratios for the Martinsburg Formation were specified as 2:1 and 10:1, respectively.

Streambed hydraulic-conductivity values (K_{str}) that range from 0.01 to 0.1 m day^{-1} were estimated for the streams in the Martinsburg Formation, springs in the carbonate rocks and seepage faces along the Potomac River (Table 4). The simulated groundwater discharge to the Potomac River from the Opequon watershed is 66,700 m^3 day^{-1} or 10.7 % of the total outflow, and compares favorably with the flow estimated by the Shenandoah Valley groundwater model (70,000 m^3 day^{-1}) of Yager et al. (2009). Estimated inflow along the western model boundary (14,400 m^3 day^{-1}) accounts for 2.5 % of the total inflow to the model domain. Simulated downward flow from carbonate rocks and upward flow along fault zones through the bottom model boundary each have the same magnitude (98,800 m^3 day^{-1}) and account for 15.9 % of the flow through the model domain (see groundwater budget in Figure 6 of ESM). The remaining inflow to the model domain (509,000 m^3 day^{-1}) is recharge, which was specified in the regression.

Three porosity values that ranged from 0.4 to 1.6 % were estimated by regression (Table 4). The largest porosity was estimated for epikarst, and the smallest porosity was estimated for the fault zones and was poorly estimated. The porosity values in the bottom two model layers were decreased using Eq. (4) and the depth coefficient λ, but were assigned a minimum value of 0.1 %. The estimated range of porosity values is similar to that estimated for the Edwards aquifer in Texas (0.1–1.3 %) by Lindgren et al. (2011). Optimum estimates of the concentration of ^{4}He entering the bottom model boundary and the ^{4}He accumulation rate were 4.9×10^{-8} ccSTP g^{-1} and 2.8×10^{-10} ccSTP g^{-1} year^{-1}, respectively. Using these values and Equation 5 of ESM, the simulated age of old water entering the model domain is 180 years, although due to the expected variability in ^{4}He accumulation rates and transit times along flow paths through the deeper parts of the aquifer (not simulated) the actual age range of old water is probably large. The ^{4}He results are discussed in the ESM.

Model fit

Comparison of observed with simulated heads and flows indicates a reasonable model fit with little bias (Fig. 11a,b). The standard error in head is 12.6 m, about 8 % of the 168-m measurement range, and most heads are within 25 m of

 DOI 10.1007/s10040-013-0997-9

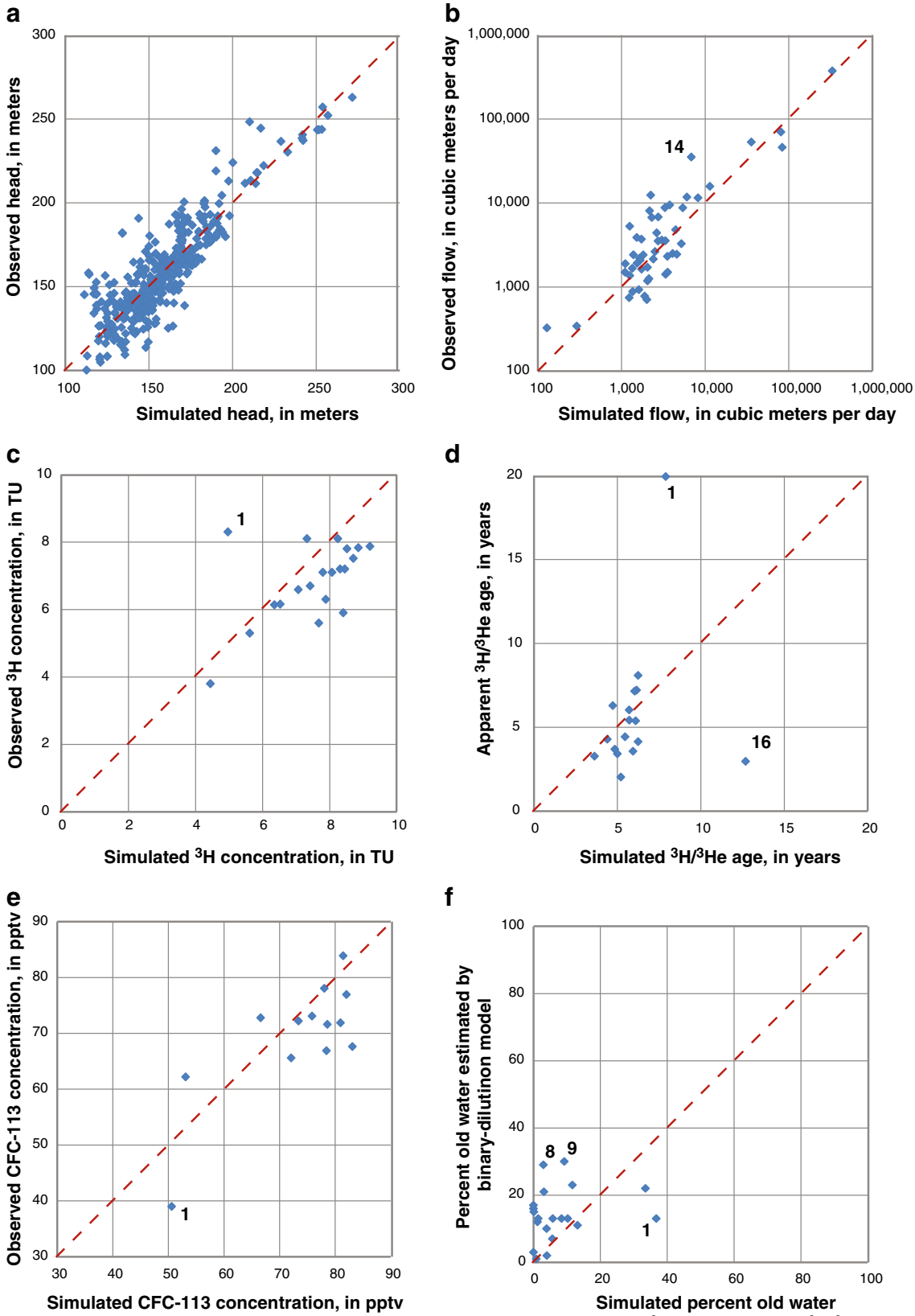

Fig. 11 Plots of simulated and observed data used in model calibration: **a** heads, **b** flows, **c** ^{3}H concentration, **d** ^{3}H/^{3}He age, **e** CFC-113 concentration, and **f** percent of old water in discharge

the observed values. In comparison, water-level fluctuations more than 25 m have been observed in some wells, so the scatter in residuals is partly the result of using single measurements from the long-term database

 DOI 10.1007/s10040-013-0997-9

in the steady-state simulation. The flow observations span 4 orders of magnitude and the median spring discharge (2,400 m^3 day^{-1}) is accurately simulated (2,500 m^3 day^{-1}). Spring discharges greater than 10,000 m^3 $day^{-1}$are under-predicted, however, including the largest discharge (35,200 m^3 day^{-1}) recorded at spring 14 (Fig. 11b). The total measured spring discharge (217,600 m^3 day^{-1}) is also under-predicted by about 30 %. This discrepancy suggests that the largest springs are better connected to the fracture network than most springs, possibly as a result of increased dissolution along conduits that convey groundwater to the springs, or that fault zones are more numerous or extensive than represented in the model.

There is more scatter in the concentration data than in either the head or flow data, partly because the relatively few measurements represent single samples from each spring. Discharges vary in both quantity and in tracer concentration at some springs, so repeated sampling (beyond the scope of this study) would be required to ensure that the data are representative of the assumed steady-state condition. The regression results fit the head, flow and concentration observations reasonably well, but there are outliers that the model simulation cannot match.

Simulated ^3H concentrations are generally larger than those observed, with the exception of spring 1 where the largest ^3H concentration measured is under-predicted (Fig. 11c). Most of the simulated $^3H/^3He$ ages agree reasonably well with the apparent $^3H/^3He$ ages (Eq. 1), with the median simulated age (5.7 years) being slightly older than the median apparent $^3H/^3He$ age (4.4 years). Although the median ages are similar, large differences in simulated and apparent ages were found for springs 1 and 16 (Fig. 11d). The simulated age for spring 1 is younger than estimated with Eq. (1) because less ^3He was produced during the short residence time in the numerical simulation. The simulated results for spring 16 are reversed, with more ^3He produced during a long residence time, yielding older ages than estimated by Eq. (1).

Both springs 1 and 16 are in the southeastern part of the model domain where the watershed boundary is close to Opequon Creek. Inspection of the simulated flow paths that discharge to spring 16 indicates that the longest flow paths originate in the Martinsburg Formation and account for most of the simulated ^3He concentration at the spring. Groundwater in the Martinsburg Formation generally has concentrations of sodium and chloride that are greater than 30 and 60 mg L^{-1}, respectively, while the water discharged by spring 16 is typical of carbonate springs in the area with less than 5 mg L^{-1} of sodium and 10 mg L^{-1} of chloride (L.N. Plummer, US Geological Survey, unpublished data, 2012). It is unlikely, therefore, that groundwater in the Martinsburg Formation is discharged at spring 16, as simulated by the numerical model. One explanation for the discrepancy in simulated ages at both springs is that the actual groundwater divide lies further to the southeast in this area than assumed. Extending the model domain to represent this condition would provide a larger recharge area up gradient of these springs, thus preventing Martinsburg water from reaching spring 16 and creating longer flow paths to spring 1.

The observed CFC-113 concentrations are matched with slight bias, although there is scatter in the data (Fig. 11e). The lowest CFC-113 concentration (measured at spring 1) is over-predicted, however, indicating less dilution with older water in the model simulation. If longer groundwater flow paths to spring 1 were simulated (by extending the model boundary to the southeast as described in the preceding), the model simulation would better match both the ^3H and CFC-113 concentrations.

Comparison of the percentages of old water in spring discharges estimated by the binary-dilution model with those simulated by the numerical model yields a poor match (Fig. 11f). The simulated percent of old water for spring 1 is larger than that estimated by the binary-dilution model, which is consistent with the conclusion that actual flow paths to the spring are longer than simulated (and would account for the larger ^3He values and the smaller ^3H values that are observed in spring discharge). The average simulated percent of old water (7.6 %) for the other springs is about one half that estimated from the binary-dilution model from concentrations of CFC-113 and tritium (14.2 %), and simulated discharges for 6 springs contain little or no old water. Although the percentages of old water calculated by the binary-dilution model could be over-estimated (see ESM) for the 6 springs using the ^3H data (including the two largest percentages, springs 8 and 9), this would only partly explain the difference in simulated results.

Discussion

Incorporating complexity in karst groundwater models

Representation of bedrock structure in the Opequon groundwater model results in a simulation that depicts anisotropic flow that is expected in folded and fractured karst terrain. Simulated flow paths converge to springs and fault zones enhance vertical flow and provide shortcuts across the bedding of carbonate rocks. The representation of these features requires detailed mapping to locate springs and develop models of geologic structure. The flow paths and travel times produced by the model provide a reasonable match to observed heads, spring discharges and concentrations of environmental tracers, and reflect the salient characteristics of the flow system.

Flow paths to springs delineated by backward particle tracking result in a complex pattern, especially in areas where springs are numerous (Fig. 12). The simulated source areas of the sampled springs reflect the effects of anisotropy and fault zones on the flow system. The bedrock structure is less complex on the west flank of the watershed and the bedding dip is shallower than on the east flank, resulting in more extensive outcrops of bedrock units with a more open pattern of folding. There is also a lower density of mapped faults on the west flank than on the east flank. The flow paths are longer and more uniform on the west flank than on the east flank. The longest flow

 DOI 10.1007/s10040-013-0997-9

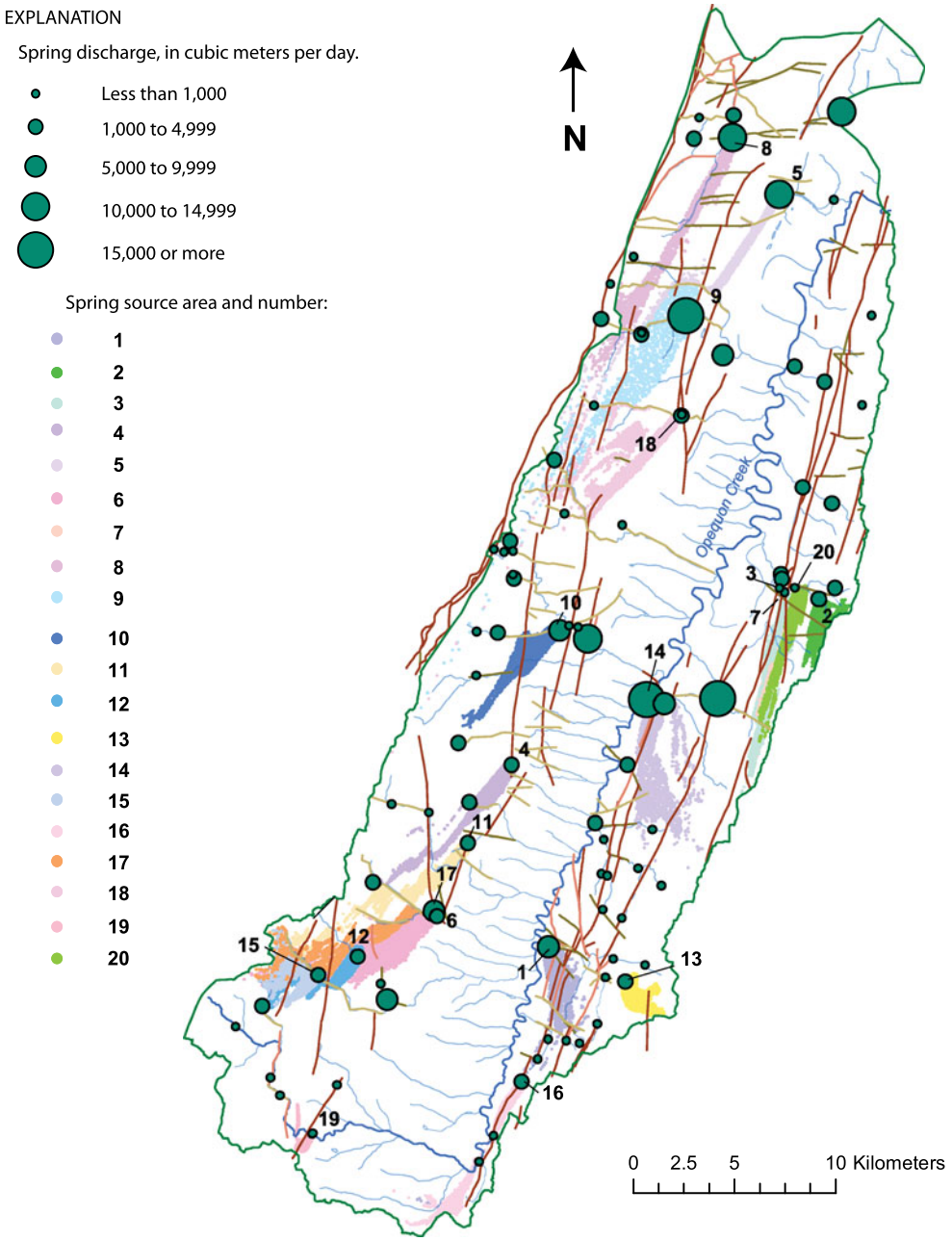

Fig. 12 Simulated source areas to sampled springs

paths (15 km) are simulated for spring 8 on the west flank and the shortest paths (less than 3 km) are simulated for spring 13 on the east flank.

Simulated groundwater transit times through the model domain also reflect the effects of anisotropy and fault zones (Fig. 13). The longest transit times (more than 20 years) are simulated for the Martinsburg Formation from groundwater mounds that form between the numerous tributaries of Opequon Creek. The shortest transit times in carbonate rocks (less than 2 years) are simulated in the vicinity of springs that are located along faults. Many stagnation zones with transit times ranging from 10 to 20 years are simulated in areas that contain few springs or faults. The mean simulated transit-times through carbonate rocks and the Martinsburg Formation are 6.7 years and 10.1 years, respectively. These transit times should be considered as conservative estimates of the flow system, since multiple groundwater ages ranging from a few days to several decades exist within the system, and mix together to provide the mean simulated transit-times.

Utility of environmental tracers in model simulations

The binary dilution model of environmental tracer data indicates that groundwater discharged from springs in the Opequon watershed can be approximated as a binary

 DOI 10.1007/s10040-013-0997-9

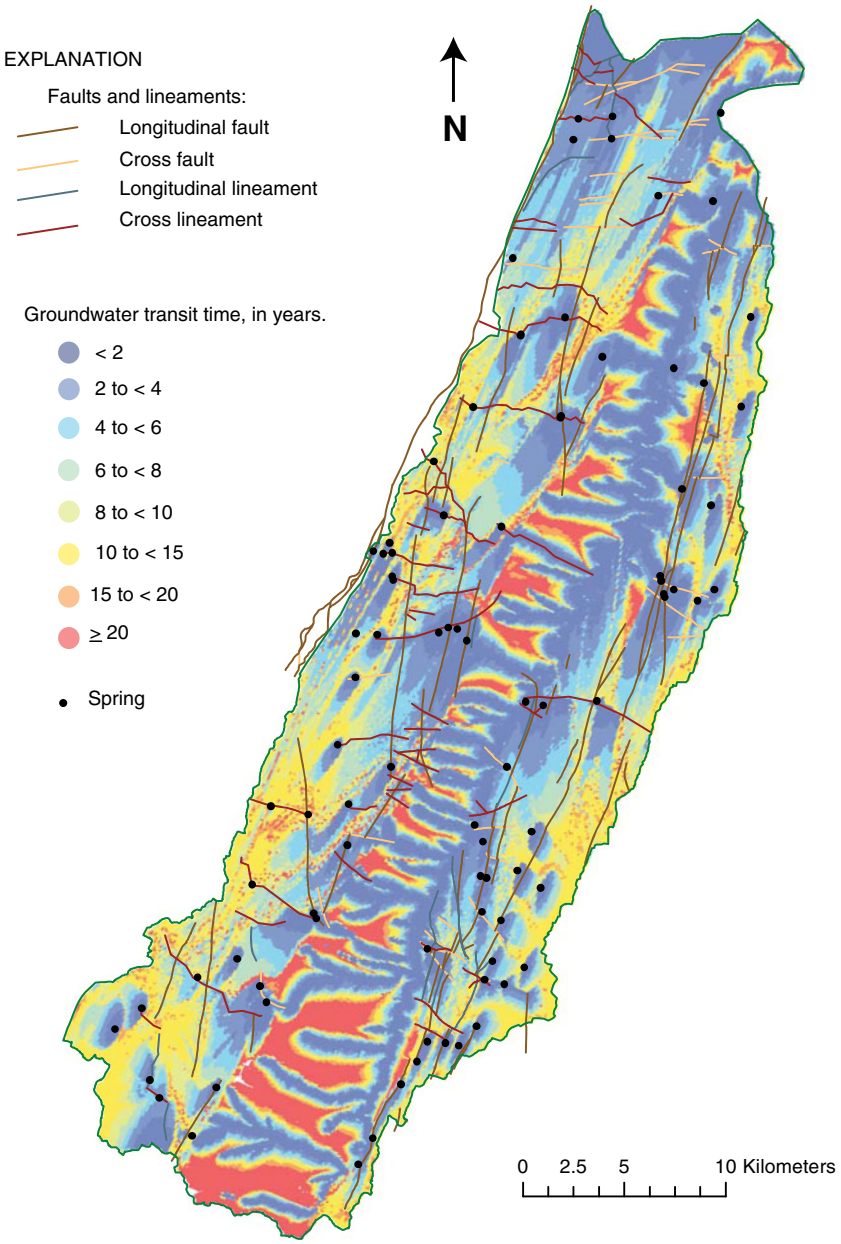

Fig. 13 Simulated groundwater transit time through model domain

mixture of young water containing ^{3}H and CFC-113, and old (tracer free) water that dilutes the environmental tracer concentrations. Numerical simulation of this condition with advective transport requires specification of upward flow of old water along fault zones at the bottom of the model domain, otherwise it is not possible to match observed ^{3}H and CFC-113 concentrations and $^{3}H/^{3}He$ ages with a single set of porosity values. Results of the binary-dilution model were instrumental in refining the initial model design because the importance of upward flow within the flow system became apparent only after these results were available.

The uncertainty in parameter estimates obtained through model calibration was greatly reduced by incorporating concentration observations derived from environmental tracers in the nonlinear regression. Including the concentration observations decreased the average value of the coefficient of variation associated with the hydraulic parameters (hydraulic conductivities and flows) from 32 to 8 %, and allowed the estimation of one additional parameter (Table 4). This reduction in uncertainty was the result of lower covariance among the parameters with the inclusion of concentration observations. The consideration of concentration observations also suggests further refinement of the model design. For example, the inability of numerical simulations to reproduce the observed ^{3}H and CFC-113 data at springs 1 and 16 indicates that the watershed boundary probably does not coincide with the groundwater divide upgradient of these springs, and that additional areas to the southeast

 DOI 10.1007/s10040-013-0997-9

also contribute additional groundwater flow to the watershed.

Model simulations allow the computation of tracer concentrations using flow-weighted averages of concentrations derived from multiple flow paths, rather than simple binary mixtures of young and old waters. The age composition of simulated spring discharge reveals that the travel times along flow paths discharging to springs generally range from less than 1 to 25 years (Fig. 14). Most of the simulated travel times are less than 10 years. The total volume of water within the model domain is about 1.5×10^9 m^3, based on porosity values estimated using the concentration observations (Table 4). This volume is equivalent to 7 years of recharge, which is consistent with the mean transit time through the carbonate rocks (6.7 years). About 44 % of the volume of stored water is within the upper 150 m of carbonate rock and 9 % is stored within the epikarst.

Limitations of model results

The Opequon groundwater-flow model is designed to simulate the diffuse flow system within the watershed that sustains perennial discharge to springs. The median spring flow is well represented, an indication that the model achieves this goal. Flow to the largest springs is under-predicted, however, either because high permeability paths created by convergent flow to these springs are not represented in the model, and/or high-conductivity zones (faults and lineaments) are more numerous or extensive than those mapped. Conduit flow through discrete karst features is not simulated, so rapid transport of tracers (for example, during dye tracing tests) or of contaminants from the land surface is not represented by the model. Although rapid movement of dye tracers with velocities in excess of 500 m day^{-1} occurs in this system, the loss of mass during dye tracing tests (as much as 90 %, e.g., Kozar et al. 2007; Doctor et al. 2011) indicates the relative importance of the diffuse flow system in the Opequon watershed.

The provenance of the old water in the Opequon watershed is uncertain. The numerical model under-predicts the percentage of old water in spring discharge relative to that estimated by the binary-dilution model, implying that either (1) deep high-conductivity faults are more numerous and extensive than presently mapped (a conclusion that is consistent with the under-prediction of

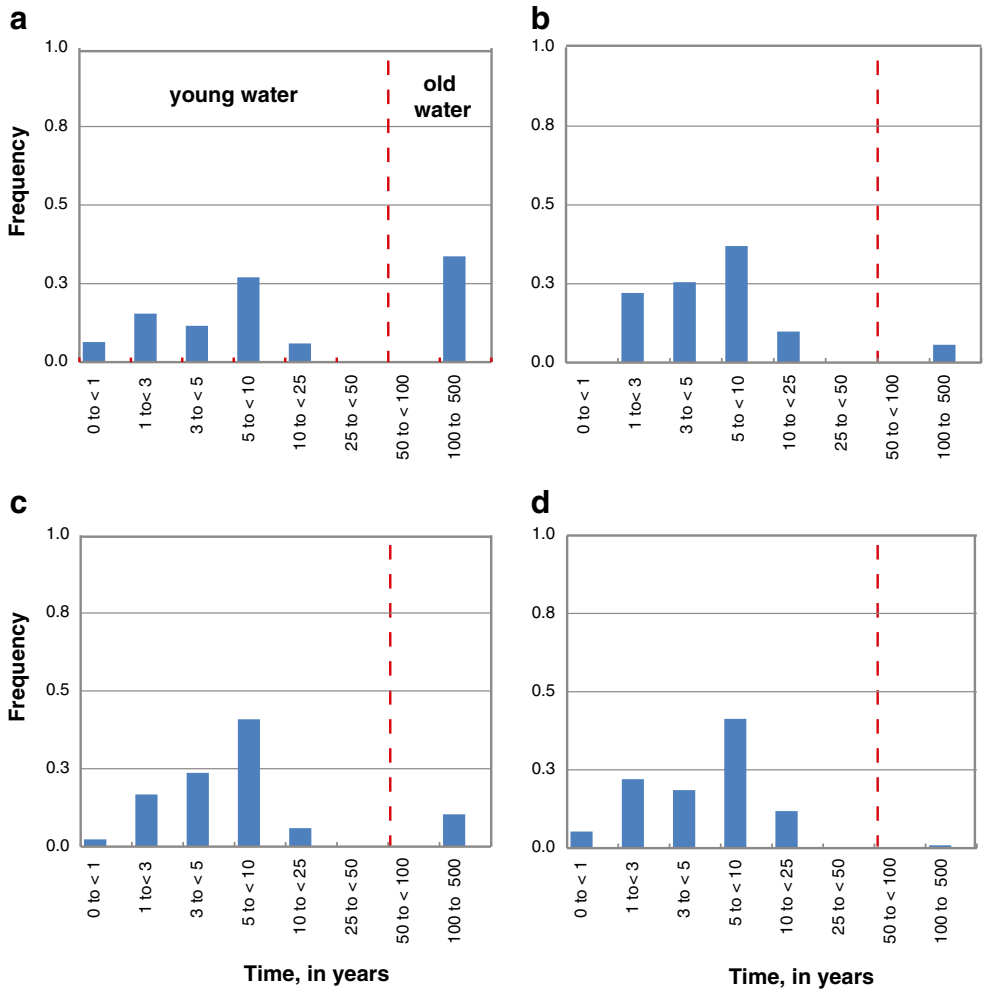

Fig. 14 Histograms showing the distribution of travel times to selected springs: **a** spring 3, **b** spring 12, **c** spring 14 and **d** spring 17

 DOI 10.1007/s10040-013-0997-9

simulated spring discharge), or (2) an additional source of old water exists within the aquifer that is not accounted for in the model (for example, old water residing in immobile zones within the carbonate rocks). An alternative 1D simulation was conducted based on equations presented in Neumann et al. (2008) to assess this possibility (see ESM). The 1D simulation represented (1) the transport of ^{3}H and ^{3}He along a flow path in the mobile zone, (2) decay of ^{3}H to ^{3}He in the mobile and immobile zones, and (3) the exchange of ^{3}H and ^{3}He between the mobile and immobile zones. The 1D simulation indicates that the exchange of young water with old water in the immobile zone cannot account for both the dilution of ^{3}H and the apparent ^{3}H/^{3}He age observed in spring discharge, assuming that the model-derived estimate of effective porosity for carbonate rock (0.9 %) is correct. Exchange between mobile and immobile water could yield the observed dilution and apparent age, but only with mobile porosity values less than 0.04 %, which would yield transit times that are more than 20 times faster than those predicted with the numerical model. The 1D simulation results are not constrained by observations of head, flow and hydraulic properties, as in the numerical model, and are, therefore, unreasonable.

A refined simulation of groundwater flow in the Opequon watershed could be constructed using a solute transport model that represents both the exchange of water between mobile and immobile domains, and upward flow of water along fault zones. In such a model, the mobile domain would represent faster flow through the connected fracture network, while the immobile domain would represent slower flow through flooded cavities and poorly connected fractures where old (tracer free) water could reside. This approach could theoretically be extended to include additional domains such as conduits and the bedrock matrix, if data were available to warrant their inclusion. Presumably, this approach would better represent the observed percentage of old water in spring discharge. Such a model would be computationally demanding, however, and require the specification of additional parameters (for example transfer coefficients between mobile and immobile domains) whose values are unknown.

The Opequon model is designed to represent a steady-state flow condition in a system that is highly dynamic. It is likely that transient flow resulting from changes in recharge could produce changes in flow paths that would affect transport of the environmental tracers examined in this study. Water levels in wells can range more than 25 m, and spring discharge can vary by an order of magnitude, causing some springs to dry up when water levels fall (G.E. Harlow, US Geological Survey, unpublished data, 2012). Such changes in flow conditions would alter flow paths to springs and, therefore, modify the mixing proportions of young and old water. For example, a higher proportion of old water is observed in some springs in the Shenandoah Valley during dry conditions when water levels are lower (Nelms and Moberg 2010). Representation of transient conditions using observed changes in heads, flows and concentrations may better estimate advective mixing within the aquifer under changing flow regimes and is the subject of an ongoing study.

The geologic structure in the Opequon watershed is reasonably well represented in the model, but an important component is missing. The dip of bedding in carbonate rocks is assumed to be vertical, but actually varies from near horizontal to vertical, and differs on the east and west flanks of the watershed. It is not possible at the present time to incorporate this feature in a MODFLOW-based model that covers a domain as large as the Opequon watershed. Alternatively, a finite-element model (such as SUTRA, see Yager et al. 2009) could be employed, but at the expense of the particle-tracking capabilities that were used in this study. In addition, detailed structure that is revealed by geologic mapping (such as the deformation of bedding that wraps around the nose of folded anticlines) is not represented in the model. A more detailed groundwater flow model could be constructed if a more refined geologic model were available, and would produce more complicated flow paths than those produced by the model discussed herein. It is important to recognize that the modeling effort described here illustrates that simulated mass balance and transit times based on environmental tracer data can be adequately described using an EPM approach, yet the individual flow paths simulated by the model do not necessarily predict actual local-scale movement of contaminants through this karst aquifer to individual springs.

Conclusions

Equivalent porous-media (EPM) models that simulate flow and advective transport such as MODFLOW and MODPATH, can be used to reproduce environmental tracer concentrations observed in spring discharge from karst aquifers that are dominated by diffuse flow. In this study, the flow system in a 915-km^2 folded and fractured karst aquifer in the Opequon watershed of the Shenandoah Valley USA was represented using an EPM model that includes anisotropy caused by bedrock structure and the influence of fault zones and springs. Groundwater in the karst aquifer flows mainly through fractured zones oriented parallel to bedding and sustains spring discharge with water that is nearly saturated with respect to calcite. The environmental-tracer data show that spring discharge can be approximated as a binary mixture of young water with a median age of 4.4 years and old (tracer-free) water. The numerical model produces a flow field in which younger water from recent recharge travels through a complex set of shallow flow paths and mixes with older water upwelling from deeper flow paths along fault zones. Tracer concentrations in simulated water mixtures discharged at model boundaries are comparable to measured concentrations of tritium, helium-3, CFC-113 and helium-4 measured in spring discharge.

Including environmental tracer concentrations in the model calibration reduced the uncertainty in estimated parameter values by a factor of four and revealed shortcomings in the initial model design. Analysis of the environmental tracer data using a binary-dilution model indicated the

 DOI 10.1007/s10040-013-0997-9

significance of vertical flow to and from the model domain, which had not previously been considered. Additional discrepancies between measured and simulated concentrations at two springs suggest that the actual groundwater divide is located southeastward of the specified model boundary. The inclusion of environmental tracer data allowed estimation of effective porosity values for the aquifer system and provided the information required to estimate the volume of water within the model domain (1.5×10^9 m^3, equivalent to about 7 years of annual recharge). The inclusion of multiple environmental-tracer concentrations in the model calibration constrained the estimated parameter values within a reasonable range.

For the Opequon watershed, the simulated median age of young water discharged from 20 springs (5.7 years) is slightly older than the apparent ^{3}H/^{3}He age (4.4 years). The simulated fraction of old water in spring discharge is 0.076, which is about one half the fraction of old water estimated by a binary-dilution model derived from measured ^{3}H and CFC-113 data. This discrepancy suggests the presence of more numerous and/or extensive zones of high hydraulic conductivity (faults and lineaments) than are presently mapped. The estimated porosity values of epikarst, carbonate rock and fault zones range from 1.5 to 0.4 % and yield a mean transit time of 6.7 years through the karst aquifer. The calibrated (K_{max}:K_{min}) anisotropy of carbonate rocks is about 20:1 and compares favorably with the value obtained through calibration of a regional groundwater-flow model of the Shenandoah Valley (17:1).

Acknowledgements Information required to construct and calibrate the groundwater flow model described in this study was provided by USGS colleagues G. Harlow, K. McCoy, J. Pope and J. Eggleston, D. Weary, and Mark Kozar. The manuscript was improved by comments from reviewers, including S. Eberts, K. McCoy, A. Massoudieh and W.P. Gardner. We thank Allen Shapiro and D. Goode who assisted with numerical simulations pertaining to the effects of exchange between mobile and immobile waters on environmental tracer concentrations. This study was supported by the USGS Groundwater Resources Program and the USGS National Research Program. Any use of trade, firm, or product names is for descriptive purposes only and does not imply endorsement by the US Government.

References

Anderman ER, Kipp KL, Hill MC, Valstar J, Neupauer RM (2002) MODFLOW-2000, the U.S. Geological Survey modular ground-water model: documentation of the Model-Layer Variable-Direction Horizontal Anisotropy (LVDA) capability of the Hydrogeologic-Unit Flow (HUF) Package. US Geol Surv Open-File Rep 02–409

Beaudoin G, Therrien R, Savard C (2006) 3D numerical modeling of fluid flow in the Val-d'Or orogenic gold district: major crustal shear zones drain fluids from overpressured vein fields. Miner Deposita 41:82–98

Bethke CM, Johnson TM (2008) Groundwater age and groundwater age dating. Annu Rev Earth Planet Sci 36:121–152

Blessent D, Therrien R, Gable CW (2011) Large-scale simulation of groundwater flow and solute transport in discretely-fractured crystalline bedrock. Adv Water Resour 34:1539–1552

Butts C (1940) Geology of the Appalachian Valley in Virginia. Part 1, Geologic text and illustrations. Virginia Geol Surv Bull 52

Cady RC (1936) Ground-water resources of the Shenandoah Valley, Virginia. Virginia Geol Surv Bull 45

Cook PG, Love AJ, Robinson NI, Simmons CT (2005) Groundwater ages in fractured rock aquifers. J Hydrol 308:284–301

Davis JH, Katz BG (2007) Hydrogeologic investigation, water chemistry analysis, and model delineation of contributing areas for City of Tallahassee public-supply wells, Tallahassee, Florida. US Geol Surv Sci Invest Rep 2007-5070

Dean SL, Kulander BR, Lessing P, Barker D (1987) Geology of the Hedgesville, Keedysville, Martinsburg, Shepherdstown, and Williamsport quadrangles, Berkeley and Jefferson Counties, West Virginia. West Virginia Geol Econ Surv Map-WV31. scale 1:24,000

Dean SL, Lessing P, Kulander BR, Barker D (1990) Geology of the Berryville, Charles Town, Harpers Ferry, Middleway, and Round Hill quadrangles, Berkeley and Jefferson Counties, West Virginia. West Virginia Geol Econ Surv Map-WV35. scale 1:24,000

Doctor DH, Orndorff W, Orndorff RC (2009) Overview of the Shenandoah Valley karst of Virginia and West Virginia. In: Stafford KW, Fratesi B (eds) Guidebook for excursion No. 1, coast to coast excursion, eastern segment, July 27 to August 5, 2009 excursion guidebook for the Fifteenth International Congress of Speleology of the International Union of Speleology. Greyhound, Huntsville, Al, pp 84–96

Doctor DH, Farrar NC, Herman JS (2011) Interaction between shallow and deep groundwater components at Fay Spring in the northern Shenandoah Valley karst. USGS Karst Interest Group Proceedings, Fayetteville, Arkansas, April 26–29. US Geol Surv Sci Invest Rep 2011-5031:25–34

Eberts SM, Bohlke JK, Kauffman LJ, Jurgens BC (2012) Comparison of particle-tracking and lumped-parameter age-distribution models for evaluating vulnerability of production wells to contamination. Hydrogeol J 20:263–282

Einsiedl F, Radke M, Maloszewski P (2010) Occurrence and transport of pharmaceuticals in a karst groundwater system affected by domestic wastewater treatment plants. J Contam Hydrol 117:26–36

Hanson RT, Kauffman LJ, Hill MC, Dickinson JE, Mehl SW (2012) Documentation of the MODPATH observation process, with support for local grid refinement and four types of observations and predictions. US Geol Surv Tech Methods 6–A42

Harbaugh AW, Banta ER, Hill MC, McDonald MG (2000) MODFLOW-2000, the US Geological Survey modular ground-water model: user guide to modularization concepts and the groundwater flow process. US Geol Surv Open-File Rep 00–92

Harlow Jr GE, Orndorff RC, Nelms DL, Weary DJ, Moberg RM (2005) Hydrogeology and ground-water availability in the carbonate aquifer system of Frederick County, Virginia. US Geol Surv Sci Invest Rep 2005-5161

Hatcher Jr RD, Thomas WA, Geiser PA, Snoke AW, Mosher S, Wiltschko DV (1989) Alleghanian orogeny. In: Hatcher RD Jr, Thomas WA, Viele GW (eds) The Appalachian-Ouachita Orogen in the United States: the geology of North America, vol F-2. Geological Society of America, Boulder, CO

Hobba Jr WA, Fisher DW, Pearson FJ Jr, Chemerys JC (1979) Hydrology and geochemistry of thermal springs of the Appalachians. US Geol Surv Prof Pap 1044-E

Hubbard DA Jr, Giannini WF, Lorah MM (1985) Travertine-marl deposits of the Valley and Ridge Province of Virginia: a preliminary report. Virginia Miner 31(1):1–16

International Atomic Energy Agency (IAEA) (2006) Use of chlorofluorocarbons in hydrology: a guidebook. STI/PUB/1238. http://www-pub.iaea.org/MTCD/publications/PDF/Pub1238_web.pdf. Accessed on 3 April 2013

International Atomic Energy Agency (IAEA) (2012) Isotope Hydrology Section, Global Network of Isotopes in Precipitation (GNIP), IAEA, Vienna. http://www-naweb.iaea.org/napc/ih/IHS_resources_gnip.html. Accessed on 3 April 2013

Jones WK, Deike GH, III (1981) A hydrogeologic study of the watershed of the National Fisheries Center at Leetown, West Virginia. Report prepared for the US Fish and Wildlife Service by Environmental Data, Frankford, WVA, 84 pp

Jones WK (1991) The carbonate aquifer of the Northern Shenandoah Valley of Virginia and West Virginia. In: Kastning EH, Kastning KM (eds) Proceedings of the Appalachian Karst Symposium, Radford VA, 23–26 March 1991, pp 217–222

Jones WK (1997) Karst hydrology atlas of West Virginia. Special Publ. no. 4, Karst Waters Institute, Charles Town, West VA

Kozar MD, Weary DJ (2009) Hydrogeology and ground-water flow in the Opequon Creek watershed area, Virginia and West Virginia. US Geol Surv Sci Invest Rep 2009-5153

Kozar MD, McCoy KJ, Weary DJ, Field MS, Pierce HA, Schill WB, Young JA (2007) Hydrogeology and water quality of the Leetown Area, West Virginia. US Geol Surv Open-File Rep 2007-1358

Lindgren RJ, Houston NA, Musgrove M, Fahlquist LS, Kauffman LJ (2011) Simulations of groundwater flow and particle-tracking analysis in the zone of contribution to a public-supply well in San Antonio, Texas. US Geol Surv Sci Invest Rep 2011-5149

Long AJ, Putnam LD (2009) Age-distribution estimation for karst groundwater: issues of parameterization and complexity in inverse modeling by convolution. J Hydrol 376:579–588

McCoy KJ, Kozar MD (2008) Use of sinkholes and specific capacity distributions to assess vertical gradients in a karst aquifer. Environ Geol 54:921–935

McCoy KJ, Podwysocki MH, Crider EA, Weary DJ (2005a) Fracture trace map and single-well aquifer test results in a carbonate aquifer in Berkeley County, West Virginia. US Geol Surv Open-File Rep 2005-1040

McCoy KJ, Podwysocki MH, Crider EA, Weary DJ (2005b) Fracture trace map and single-well aquifer test results in a carbonate aquifer in Jefferson County, West Virginia. US Geol Surv Open-File Rep 2005-1407

Michel RL (1989) Tritium deposition over the continental United States, 1953–1983. In: Delleur JW (ed) Atmospheric deposition. International Association of Hydrological Sciences, Wallingford, UK, pp 109–115

Nelms DL, Moberg RM (2010) Hydrogeology and groundwater availability in Clarke County, Virginia. US Geol Surv Sci Invest Rep 2010-5112

Nelms DL, Harlow GE Jr, Hayes DC (1997) Base-flow characteristicsof streams in the Valley and Ridge, the Blue Ridge, andthe Piedmont physiographic provinces of Virginia. US Geol Surv Water Suppl Pap 2457

Neumann RB, LaBolle EM, Harvey CF (2008) The effects of dual-domain mass transfer on the tritium-helium-3 dating method. Environ Sci Technol 42:4837–4843

Perry LD, Costain JK, Geiser PA (1979) Heat flow in western Virginia and a model for the origin of thermal springs in the folded Appalachians. J Geophys Res 84(B12):6875–6883

Poeter EP, Hill MC (1998) Documentation of UCODE, A computer code for universal inverse modeling. US Geol Surv Water Res Invest Rep 98-4080

Poeter EP, Hill MC, Banta ER, Mehl, S, Christensen S (2005) UCODE_2005 and six other computer codes for universal sensitivity analysis, calibration, and uncertainty evaluation. US Geol Surv Tech Methods 6-A11

Pollock D (1994) User's guide for MODPATH/MODPATH-PLOT, version 3: a particle tracking post-processing package for MODFLOW, the U. S. Geological Survey finite-difference ground-water flow model. US Geol Surv Open-File Rep 94-464

Sanford WE, Plummer LN, McAda DP, Bexfield LM, Anderholm SK (2004) Hydrochemical tracers in the Middle Rio Grande Basin, USA: 2. calibration of a ground-water flow model. Hydrogeol J 12(4):389–407

Sanford W (2011) Calibration of models using groundwater age. Hydrogeol J 19:13–16

Scanlon BR, Mace RE, Barrett ME, Smith B (2003) Can we simulate regional groundwater flow in a karst system using equivalent porous media models? Case study, Barton Springs Edwards aquifer, USA. J Hydrol 276:137–158

Schlosser P, Stute M, Dorr H, Sonntag C, Munnich KO (1988) Tritium/^{3}He dating of shallow groundwater. Earth Planet Sci Lett 89:353–362

Schlosser P, Stute M, Dorr H, Sonntag C, Munnich KO (1989) Tritiogenic ^{3}He in shallow groundwater. Earth Planet Sci Lett 94:245–256

Senior LA, Goode DJ (1999) Ground-water system, estimation of aquifer hydraulic properties, and effects of pumping on ground-water flow in Triassic sedimentary rocks in and near Lansdale, Pennsylvania. US Geol Surv Water Res Invest Rep 99-4228

Shapiro AM (2001) Effective matrix diffusion in kilometer-scale transport in fractured crystalline rock. Water Resour Res 37(3):507–522

Shapiro AM (2011) The challenge of interpreting environmental tracer concentrations in fractured rock and carbonate aquifers. Hydrogeol J 19:9–12

Schuster ET, White WB (1971) Seasonal fluctuations in the chemistry of limestone springs: a possible means for characterizing carbonate aquifers. J Hydrol 14:93–128

Solomon DK, Genereux DP, Plummer LN, Busenberg E (2010) Testing mixing models of old and young groundwater in a tropical lowland rain forest with environmental tracers. Water Resour Res 46, W04518. doi:10.1029/2009WR008341

Tiedeman CR, Lacombe PJ, Goode DJ (2010) Multiple well-shutdown tests and site-scale flow simulation in fractured rocks. Ground Water 48(3):401–415

Therrien R, Sudicky EA (1996) Three-dimensional analysis of variably-saturated flow and solute transport in discretely fractured porous media. J Contam Hydrol 23:1–44

Trapp H, Jr, Horn MA (1997) Ground Water Atlas of the United States, Delaware, Maryland, New Jersey, North Carolina, Pennsylvania, Virginia, West Virginia. US Geol Surv Hydrol Atlas HA 730-L

Troldberg L, Jensen KH, Engesgaard P, Refsgaard JC, Hinsby K (2008) Using environmental tracers in modeling flow in a complex aquifer system. J Hydrol Eng 13(11):1037–1048

US Department of Commerce (2012) National Oceanic and Atmospheric Administration (NOAA), Earth System Research Laboratory, Global Monitoring Division, Boulder, CO, USA. Available at http://www.esrl.noaa.gov/gmd/. Accessed on 3 April 2012

US Department of Energy (2012) DOE, Carbon Dioxide Information Analysis Center (CDIAC). Oak Ridge National Laboratory (ORNL), Oak Ridge, TN, USA. Available at http://cdiac.esd.ornl.gov/. Accessed on 3 April 2013

US Geological Survey (2012) US Geological Survey, Reston Chlorofluorocarbon Laboratory. US Geological Survey, Reston, VA. Available at http://water.usgs.gov/lab/chlorofluorocarbons/sampling/.Accessed on 3 April 2013

Weary DJ (2008) Preliminary Map of potentially karstic carbonate rocks in the central and southern Appalachian states. US Geol Surv Open-File Rep 2008-1154

Weissmann GS, Zhang Y, LaBolle EM, Fogg GE (2002) Dispersion of groundwater age in an alluvial aquifer system. Water Res Res 38(10):1198–1211

Worthington SRH (2009) Diagnostic hydrogeologic characteristics of a karst aquifer (Kentucky, USA). Hydrogeol J 17:1665–1678

Wright WG (1990) Groundwater hydrology and quality in the Valley and Ridge and Blue Ridge physiographic provinces of Clarke County, Virginia, US Geol Surv Water Res Invest Rep 90-4134

Wu Q, Zhou W, Pan G, Ye S (2009) Application of a discrete-continuum model to karst aquifers in North China. Ground Water 47(3):453–461

Yager RM (1996) Simulated three-dimensional ground-water flow in the Lockport Group, a fractured-dolomite aquifer near Niagara Falls, New York. US Geol Surv Water Supply Pap 2487

Yager RM, Ratcliffe NM (2010) Hydrogeology and simulation of groundwater flow in fractured rock in the Newark Basin, Rockland County, New York. US Geol Surv Sci Invest Rep 2010-5250

Yager RM, Voss CI, Southworth S (2009) Comparison of alternative representations of hydraulic-conductivity anisotropy in folded fractured-sedimentary rock: modeling groundwater flow in the Shenandoah Valley (USA). Hydrogeol J 17(5):1111–1131

Zheng C, Bennett GD (2002) Applied contaminant transport modeling. Wiley, New York